

Continual Deep Learning by Functional Regularisation of Memorable Past

Pingbo Pan^{*1} Siddharth Swaroop^{*2} Alexander Immer³ Runa Eschenhagen⁴ Richard E. Turner²
 Mohammad Emtiyaz Khan⁵

Abstract

Continually learning new skills is important for intelligent systems, yet most deep learning methods suffer from catastrophic forgetting of the past. Recent works address this with weight regularisation. Functional regularisation, although computationally expensive, is expected to perform better, but rarely does so in practice. In this paper, we fix this issue by proposing a new functional-regularisation approach that utilises a few *memorable past* examples that are crucial to avoid forgetting. By using a Gaussian Process formulation of deep networks, our approach enables training in weight-space while identifying both the memorable past and a functional prior. Our method achieves state-of-the-art performance on standard benchmarks and opens a new direction for life-long learning where regularisation and memory-based methods are naturally combined.

1. Introduction

The ability to quickly adapt to changing environments is an important quality of intelligent systems. For such quick adaptation, it is important to be able to identify, memorise, and recall useful past experiences when acquiring new ones. Unfortunately, standard deep-learning methods are not good at maintaining previously acquired skills, and can quickly forget them when learning new skills (Kirkpatrick et al., 2017). Such catastrophic forgetting presents a big challenge for applications, such as robotics, where new tasks can appear during training, and data from previous tasks might be unavailable for retraining.

In recent years, many methods have been proposed to ad-

^{*}Equal contribution ¹University of Technology Sydney, Australia ²University of Cambridge, UK ³EPFL, Switzerland ⁴University of Tbingen, Germany ⁵RIKEN Center for AI project, Japan. ^{1,3,4}Work done during an internship at RIKEN Center for AI Project, Japan. Correspondence to: Emtiyaz Khan <emtiyaz.khan@riken.jp>, Siddharth Swaroop <ss2163@cam.ac.uk>.

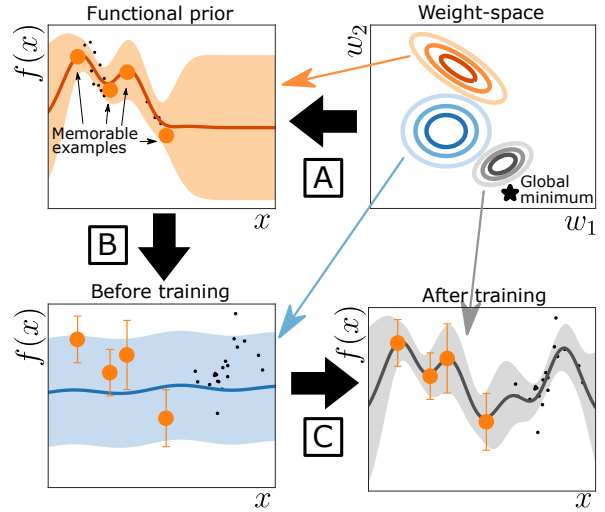


Figure 1. Our method consists of three main steps. In Step A, we convert the previously trained network (orange ellipses) to a Gaussian process (top left) which is then used as a “functional prior” to regularise the next task. In step B, we choose a few memorable past examples (orange circles) that are crucial to avoid forgetting. In step C, we train a new network over the next task (black dots in the bottom row) while making sure that the predictions over memorable past examples remain unchanged. All these steps are carried out using the framework of Khan et al. (2019).

dress catastrophic forgetting in deep learning. One of the most popular approaches is to keep the network weights close to the values obtained for the previous tasks/data (Kirkpatrick et al., 2017; Nguyen et al., 2018; Zenke et al., 2017; Ebrahimi et al., 2019; Serra et al., 2018). However, this may not always ensure that the predictions on previous tasks also remain unchanged. Since the network outputs depend on the weights in a complex way, such *weight-regularisation* may not be effective.

A better approach is to use *functional-regularisation*, where we directly regularise the network outputs (Benjamin et al., 2018), but this is costly because it requires the derivatives of outputs at many input locations. Existing approaches reduce these costs by carefully selecting the locations, e.g. by using *working memory* (Benjamin et al., 2018) or Gaussian-Process inducing points (Titsias et al., 2019), but currently these methods do not consistently outperform existing weight-regularisation methods.

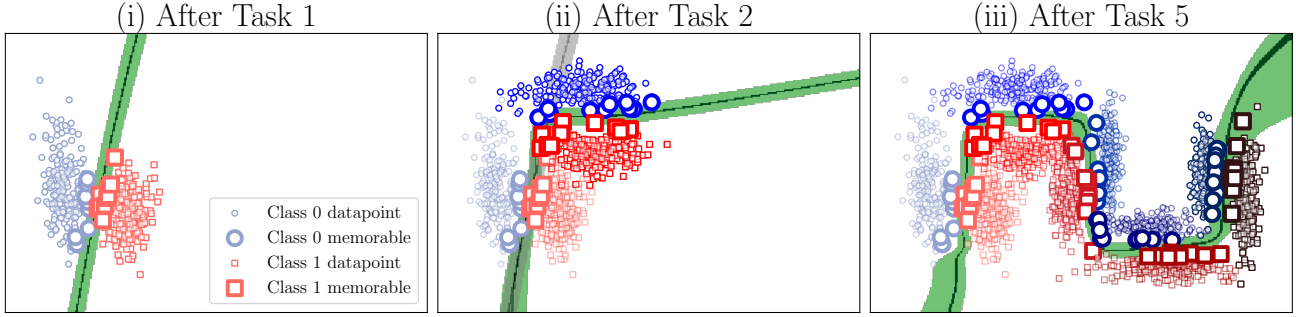


Figure 2. This figure demonstrates our approach on a toy dataset. Figure (i) shows the result of training on the first task where memorable past examples are shown with big markers. These points usually are the ones that support the decision boundary. Figure (ii) shows the result after training on the second task where we see that the new network outputs are forced to give the same prediction on memorable past examples as the previous network. The new decision boundary classifies both task 1 and 2 well. Figure (iii) shows the result after training on five tasks, along with the memorable-past of each task. With our method, the performance over past tasks is maintained.

To fix this issue, we propose a new functional-regularisation method called Functional Regularisation of Memorable Past (FROMP). Our key idea is to regularise the network outputs at a few *memorable past* examples that are crucial to avoid forgetting. Figure 1 illustrates the three main steps of our method: (A) convert previously trained networks as *functional priors* to regularise new tasks; (B) identify memorable past examples crucial to avoid forgetting; and (C) train in the weight-space while regularising in function-space. All three steps are carried out using a single framework based on the method of Khan et al. (2019). Our method achieves state-of-the-art performance on standard benchmarks, and is consistently better than both the existing weight-regularisation and functional-regularisation methods. A toy example is shown in Figure 2. Our work in this paper focuses on avoiding forgetting, but it also opens a new direction for life-long learning methods where regularisation methods are naturally combined with memory-based methods.

1.1. Related Works

Our goal is to consistently outperform weight-regularisation. With our method, we fix many issues with the existing functional-regularisation methods. Unlike Benjamin et al. (2018), our method has a mechanism to automatically weight past memory and also estimate uncertainty. Unlike GP-based methods, it does not require specification of a kernel, and unlike Titsias et al. (2019), it does not require optimisation of input locations. Both of these are obtained using the method of Khan et al. (2019). The kernel obtained is closely related to the Neural Tangent Kernel (NTK) (Jacot et al., 2018), but does not require infinite-width assumptions.

Our method consistently outperforms many existing weight and functional regularisation approaches. The method proposed by Titsias et al. (2019) is also promising, but unlike our method it performs worse than the weight-regularisation method of Swaroop et al. (2019). We also obtain state-of-

the-art performance on a larger split CIFAR benchmark. This comparison is missing in Titsias et al. (2019).

Our method is based on a set of memorable past examples. Many such memory-based approaches exist (Rebuffi et al., 2017; Shin et al., 2017; Aljundi et al., 2019; Chaudhry et al., 2019; Lopez-Paz & Ranzato, 2017; Chaudhry et al., 2018). Compared to these approaches, an advantage of our method is that the memory is obtained within the functional-regularisation framework and does not require solving a different optimisation problem. The computation is also straightforward, simply requiring a forward-pass through the network followed by sorting (see Section 3.2).

Broadly, existing work on continual learning can be split into three approaches: inference-based, memory/rehearsal-based, and model-based. There have also been hybrid approaches attempting to combine them. Inference-based approaches have mostly focused on weight regularisation, with some recent efforts on functional regularisation. Our work falls in the latter category, but is also closely related to memory-based approaches.

2. Continual Learning with Weight/Functional Regularisation

In deep learning, we minimise loss functions to estimate network weights. For example, in supervised multi-class classification problems, we are given a dataset \mathcal{D} of N input-output pairs with outputs \mathbf{y}_i , a one-hot encoded vector of K classes, and inputs \mathbf{x}_i , a vector of length D . Our goal is to minimise a loss which takes the following form: $N\bar{\ell}(\mathbf{w}) + \delta R(\mathbf{w})$, where $\bar{\ell}(\mathbf{w}) := \frac{1}{N} \sum_{i=1}^N \ell(\mathbf{y}_i, \mathbf{f}_w(\mathbf{x}_i))$ with deep neural network $\mathbf{f}_w(\mathbf{x}) \in \mathbb{R}^K$ and its weights $\mathbf{w} \in \mathbb{R}^P$, $\ell(\mathbf{y}, \mathbf{f})$ denotes a differentiable loss function between an output \mathbf{y} and the network output \mathbf{f} , $R(\mathbf{w})$ is a regularisation function (usually an L_2 -regulariser $R(\mathbf{w}) := \mathbf{w}^\top \mathbf{w}$), and $\delta > 0$ controls the regularisation strength. Standard deep-

learning approaches rely on an unbiased stochastic-gradient of the loss $\bar{\ell}$. This usually requires an ability to access all of the data examples for all classes throughout training (Bottou, 2010). It is this unbiased, minibatch setting where deep-learning excels and achieves state-of-the-art performance on many benchmark datasets.

In reality, we do not always have access to all the data at once, and it is not possible to obtain unbiased stochastic gradients. New classes may appear during training and old classes may never be seen again. For such settings, vanilla mini-batch stochastic-gradient methods lead to catastrophic forgetting of past information (Kirkpatrick et al., 2017). Our goal in this paper is to design methods that can avoid such catastrophic forgetting. We focus on a particular setting where the classification task is divided into several tasks, e.g., a task may consist of a classification problem over a subset of classes. We assume that the tasks arrive sequentially one after the other. Once the learning is over, we may never see that task again. Such continual-learning settings have been considered in previous works (Kirkpatrick et al., 2017; Nguyen et al., 2018; Zenke et al., 2017), and our goal is to avoid forgetting of old tasks in this setting.

Recent methods have proposed weight-regularisation as a way to combat catastrophic forgetting. The main idea is to keep the new network weights close to the old ones, e.g., when training on the task t while given network weights \mathbf{w}_{t-1} trained on previous tasks 1 to $t-1$, we can minimise the following loss: $N\bar{\ell}_t(\mathbf{w}) + \delta(\mathbf{w} - \mathbf{w}_{t-1})^\top \mathbf{F}_{t-1}(\mathbf{w} - \mathbf{w}_{t-1})$, where $\bar{\ell}_t(\mathbf{w})$ is the loss defined over all data examples from task t and \mathbf{F}_{t-1} is a preconditioning matrix that favours the weights relevant to the past tasks more than the rest. The Elastic-Weight Consolidation (EWC) method (Kirkpatrick et al., 2017), for example, uses the Fisher information matrix as the pre-conditioner, while Ritter et al. (2018) use the Hessian of the loss, and variational continual learning (VCL) (Nguyen et al., 2018) employs the precision matrix of the variational approximation. To reduce complexity, usually a diagonal (or block diagonal) matrix is used. Such weight-space methods reduce forgetting but do not produce satisfactory results.

The challenge in using weight-regularisation lies in the fact that the exact values of the weights do not really matter due to parametric symmetries (Benjamin et al., 2018; Bishop, 2006). Making current weights closer to the previous ones may not always ensure that the predictions on the previous tasks also remain unchanged. Since the network outputs depend on the weights in a complex way, it is difficult to ensure the effectiveness of *weight-regularisation*.

A better approach is to directly regularise the outputs, because what matters is the network output, not the values of the weights. For example, similar to Benjamin et al. (2018), we can use an L_2 -regulariser over the function values on

data examples from past tasks:

$$\min_{\mathbf{w}} N\bar{\ell}_t(\mathbf{w}) + \delta \sum_{s=1}^{t-1} (\mathbf{f}_{t,s} - \mathbf{f}_{t-1,s})^\top (\mathbf{f}_{t,s} - \mathbf{f}_{t-1,s}), \quad (1)$$

where $\mathbf{f}_{t,s}$ and $\mathbf{f}_{t-1,s}$ are vectors of function values $f_w(\mathbf{x}_i)$ and $f_{w_{t-1}}(\mathbf{x}_i)$ respectively for all $i \in \mathcal{D}_s$ with \mathcal{D}_s being the dataset for the task s . Rather than making the weights \mathbf{w} similar to \mathbf{w}_{t-1} , such *functional-regularisation* approaches directly force the function values to be similar. Because of this, we expect them to perform better than weight-regularisation. This is also expected to happen when taking a Bayesian approach where posterior approximations in the function-space might be better than those in the weight-space.

Unfortunately, functional-regularisation is computationally infeasible because it requires us to store all past data and compute function values over them. This computational issue is typically solved by choosing only a few input locations. Benjamin et al. (2018) employ a *working memory* (Lopez-Paz & Ranzato, 2017; Rebuffi et al., 2017) while Titsias et al. (2019) use the inducing point method based on a Gaussian process framework. As discussed earlier, both of these approaches have issues. Most importantly, these methods do not consistently outperform the existing weight-regularisation methods. This could be due to the methods they use to build memory or enforce functional regularisation. Our goal in this paper is to design a functional-regularisation method that is consistently better than weight-regularisation. We build upon the method of Khan et al. (2019) to convert deep networks into Gaussian processes, which we describe next.

3. Functional-Regularisation of Memorable Past (FROMP)

We will now describe the three main steps of our method which are illustrated in Figure 1.

3.1. From Deep Networks to Functional Priors

Khan et al. (2019) propose an approach called DNN2GP to convert deep networks to Gaussian processes (GPs). In step A, we employ such GPs as functional priors to regularise the next task.

The DNN2GP approach is very similar to the standard weight-space to function-space conversion for linear basis-function models (Rasmussen & Williams, 2006). For example, consider a linear regression model on a scalar output $y_i = f_w(\mathbf{x}_i) + \epsilon_i$ with a function output $f_w(\mathbf{x}_i) := \phi(\mathbf{x}_i)^\top \mathbf{w}$ using a feature map $\phi(\mathbf{x})$. Assume Gaussian noise $\mathcal{N}(\epsilon_i|0, \Lambda^{-1})$ and a Gaussian prior $\mathcal{N}(\mathbf{w}|0, \delta^{-1}\mathbf{I}_P)$ where \mathbf{I}_P is the identity matrix of size $P \times P$. It can then be shown that the posterior distribution of this linear model, denoted by $\mathcal{N}(\mathbf{w}|\mathbf{w}_{\text{lin}}, \Sigma_{\text{lin}})$, induces a GP posterior on function $f_w(\mathbf{x})$

whose mean and covariance functions are given as follows (Appendix A.1 or Rasmussen & Williams (2006) Chapter 2):

$$m_{\text{lin}}(\mathbf{x}) := f_{w_{\text{lin}}}(\mathbf{x}), \quad \kappa_{\text{lin}}(\mathbf{x}, \mathbf{x}') := \boldsymbol{\phi}(\mathbf{x})^\top \boldsymbol{\Sigma}_{\text{lin}} \boldsymbol{\phi}(\mathbf{x}'), \quad (2)$$

where w_{lin} is simply the Maximum A Posteriori (MAP) estimate of the linear model, and

$$\boldsymbol{\Sigma}_{\text{lin}}^{-1} := \sum_i \boldsymbol{\phi}(\mathbf{x}_i) \Lambda \boldsymbol{\phi}(\mathbf{x}_i)^\top + \delta \mathbf{I}_P. \quad (3)$$

DNN2GP computes a similar GP posterior for a neural network when the posterior is approximated by a Gaussian. Given a local minimum \mathbf{w}_* of the loss $N\ell(\mathbf{w}) + \delta \mathbf{w}^\top \mathbf{w}$ for a scalar output $f_w(\mathbf{x})$, we can construct a Gaussian approximation via the Laplace approximation. We use an approximation with mean $\boldsymbol{\mu}_* = \mathbf{w}_*$ and covariance

$$\boldsymbol{\Sigma}_*^{-1} = \sum_{i=1}^N \mathbf{J}_{w_*}(\mathbf{x}_i)^\top \Lambda_{w_*}(\mathbf{x}_i, y_i) \mathbf{J}_{w_*}(\mathbf{x}_i) + \delta \mathbf{I}_P, \quad (4)$$

where $\Lambda_{w_*}(\mathbf{x}, y) := \nabla_{\text{ff}}^2 \ell(y, f)$ is the scalar Hessian of the loss function, and $\mathbf{J}_{w_*}(\mathbf{x}) := \nabla_w f_w(\mathbf{x})^\top$ is the $1 \times P$ Jacobian of the network, all evaluated at $\mathbf{w} = \mathbf{w}_*$. This corresponds to a Gauss-Newton approximation. Comparing Equations 3 and 4, we can interpret $\boldsymbol{\Sigma}_*$ as the covariance of a linear model with a feature map $\mathbf{J}_{w_*}(\mathbf{x})^\top$ and noise precision $\Lambda_{w_*}(\mathbf{x}, y)$. Using this similarity to the linear model, it is possible to derive a GP posterior approximation for neural networks.

Khan et al. (2019) derive this for a generic loss function (see Appendix B2 in their paper), e.g., for a regression loss, the mean and covariance functions of the GP posterior take the following form:

$$m_{w_*}(\mathbf{x}) := f_{w_*}(\mathbf{x}), \quad \kappa_{w_*}(\mathbf{x}, \mathbf{x}') := \mathbf{J}_{w_*}(\mathbf{x}) \boldsymbol{\Sigma}_* \mathbf{J}_{w_*}(\mathbf{x}')^\top. \quad (5)$$

This is equivalent to Equation 2 if we set the feature map $\boldsymbol{\phi}(\mathbf{x}) \equiv \mathbf{J}_{w_*}(\mathbf{x})^\top$. A similar equation holds for other loss functions such as those used for binary and multiclass classification. Exact expressions and detailed derivations are given in Appendix A.2. We denote such GP posteriors by $\mathcal{GP}(m_{w_*}(\mathbf{x}), \kappa_{w_*}(\mathbf{x}, \mathbf{x}'))$, and use them as a *functional prior* to regularise the next task.

The above result holds at a minimiser \mathbf{w}_* , but can be extended to a sequence of weights obtained during optimisation. Khan et al. (2019) show this for a variational-inference algorithm to obtain Gaussian approximations. Given such approximations, we can obtain GPs by first sampling \mathbf{w} and replacing \mathbf{w}_* by \mathbf{w} in Equation 5. We denote the resulting GP by $\mathcal{GP}(m_w(\mathbf{x}), \kappa_w(\mathbf{x}, \mathbf{x}'))$. The result also applies to variants of Newton’s method and RMSprop. More details are in Appendix A.3.

Khan et al. (2019) discuss the relationship of the GP posterior to the Neural Tangent Kernel (NTK) (Jacot et al., 2018). The prior distribution to obtain the posterior in Equation 5 corresponds to the NTK at finite width. A slightly different kernel is obtained when a variational approximation is used.

3.2. Identifying Memorable past

We now describe selection of a few memorable past examples to reduce the computation cost. Fortunately, this can be done within the DNN2GP approach by exploiting a property of linear models. Consider a linear model where different noise precision Λ_i is assigned to each pair $\{\mathbf{x}_i, y_i\}$. For MAP estimation, the examples with high value of Λ_i contribute more, as is clear from the objective shown below:

$$\mathbf{w}_{\text{MAP}} = \arg \max_{\mathbf{w}} \sum_{i=1}^N \Lambda_i (y_i - \boldsymbol{\phi}(\mathbf{x}_i)^\top \mathbf{w})^2 + \delta \mathbf{w}^\top \mathbf{w}. \quad (6)$$

The noise precision Λ_i can therefore be interpreted as the relevance of the data example i . Such relevant examples are crucial to ensure that the solution stays at \mathbf{w}_{MAP} or close to it. These ideas are widely used in the theory of leverage-score sampling (Alaoui & Mahoney, 2015; Ma et al., 2015), where datapoints are picked proportional to the leverage score. We use this idea to ensure that the solution obtained on the next task remains close to the previous one.

We do this via the DNN2GP approach, which gives us a linear model with different noise precisions for each data example. We can see this by inspecting Equations 3 and 4, where the quantity $\Lambda_{w_*}(\mathbf{x}_i, y_i)$ plays the same role as the noise precision Λ . Therefore, $\Lambda_{w_*}(\mathbf{x}_i, y_i)$ can be used as a relevance measure, and a simple approach to pick memorable examples is to sort it $\forall i$ and pick the top few examples as the memorable examples. This simple solution is effective because $\Lambda_{w_*}(\mathbf{x}_i, y_i)$ are obtained from \mathbf{w}_* , and therefore reflect the relevance of the data examples to maintain this solution. An example is shown in Figure 2: our approach clearly picks examples close to the decision boundary.

The quantity $\Lambda_{w_*}(\mathbf{x}_i, y_i)$ is extremely cheap to compute as it is simply the second derivative of the loss. This can be obtained with a forward pass to get $\ell(y_i, \hat{y}_i)$, followed by double differentiation with respect to \hat{y}_i . We refer to examples chosen by this method as *memorable past* examples. After training on every task, we select a few memorable examples in \mathcal{D}_t , denoting the set of such examples by \mathcal{M}_t .

3.3. Training in weight-space with a functional prior

We will now describe the final step of our algorithm, which enables us to train in weight space while regularising in function space. To do so, we use the Bayesian formulation of continual learning, where we replace the prior distribution in weight space by the functional prior. Then by employing algorithmic approximations, we will get a functional-regularisation method which is an improved version of Equation 1.

Given a loss of the form $N\bar{\ell}_t(\mathbf{w}) + R(\mathbf{w})$, a Bayesian formulation in weight-space employs a regulariser that uses the previous posterior distribution, i.e., $R(\mathbf{w}) \equiv -\log p(\mathbf{w}|\mathcal{D}_{1:t-1})$.

Computing the exact posterior distribution, or a tempered version of it, would in theory avoid catastrophic forgetting. However, the exact posterior is difficult to compute, and we are forced to use approximations, e.g., [Nguyen et al. \(2018\)](#) use the variational approximation from the previous task $q_{t-1}(\mathbf{w}) \approx p(\mathbf{w}|\mathcal{D}_{1:t-1})$ as the weight regulariser. The resulting Bayesian objective can be written as follows,

$$\min_{q(\mathbf{w})} \mathbb{E}_{q(\mathbf{w})} \left[\frac{N}{\tau} \bar{\ell}_t(\mathbf{w}) + \log q(\mathbf{w}) - \textcolor{red}{\log q_{t-1}(\mathbf{w})} \right], \quad (7)$$

where the last term is the weight regulariser, and τ is a tempering parameter. By using a Gaussian approximation $q(\mathbf{w}) = \mathcal{N}(\mathbf{w}|\boldsymbol{\mu}, \boldsymbol{\Sigma})$, this amounts to optimising for $\{\boldsymbol{\mu}, \boldsymbol{\Sigma}\}$. Unfortunately, such approximate Bayesian methods in weight-space are less effective in avoiding catastrophic forgetting. Our goal is to use a function-space formulation of this objective using GP posteriors derived in Section 3.1.

Ideally, we might want to transform the whole objective into function-space, but this might be computationally challenging. A more feasible alternative is to only replace the weight regulariser (the last term, shown in red) by a functional one. The regulariser is an integral $\int q(\mathbf{w})[\log q_{t-1}(\mathbf{w})] d\mathbf{w}$ in weight-space, and we can replace it by an integral in function-space using a change of variable from \mathbf{w} to $f_{\mathbf{w}}$, the network output. Specifically, we will replace both $q(\mathbf{w})$ and $q_{t-1}(\mathbf{w})$ by their functional counterparts obtained in Section 3.1. To reduce computational costs, the integral is evaluated only at the function outputs obtained at the memorable past examples.

Denoting a sample from $q(\mathbf{w})$ by \mathbf{w}_t , we can substitute this sample into Equation 5, giving us a GP posterior. We denote this by $\tilde{q}_{\mathbf{w}_t}(\mathbf{f}) = \mathcal{N}(\mathbf{f}|\mathbf{m}_t, \mathbf{K}_t)$, where \mathbf{f} denotes the vector of function values defined at memorable past examples $\bigcup_{s=1}^{t-1} \mathcal{M}_s$, and \mathbf{m}_t and \mathbf{K}_t respectively denote the mean vector and kernel matrix obtained by evaluating $\mathcal{GP}(m_{\mathbf{w}_t}(\mathbf{x}), \kappa_{\mathbf{w}_t}(\mathbf{x}, \mathbf{x}'))$ at the memorable past examples. Similarly, denoting a sample from $q_{t-1}(\mathbf{w})$ by \mathbf{w}_{t-1} , we can obtain another GP posterior, which we denote by $\tilde{q}_{\mathbf{w}_{t-1}}(\mathbf{f}) = \mathcal{N}(\mathbf{f}|\mathbf{m}_{t-1}, \mathbf{K}_{t-1})$. This posterior is used as the functional prior for the next task.

Using these GPs, we approximate the integral in weight-space by an integral in function-space as follows:

$$\begin{aligned} \mathbb{E}_{q(\mathbf{w})}[\log q_{t-1}(\mathbf{w})] &\approx \mathbb{E}_{\tilde{q}_{\mathbf{w}_t}(\mathbf{f})}[\log \tilde{q}_{\mathbf{w}_{t-1}}(\mathbf{f})] \\ &= -\frac{1}{2} [\text{Tr}(\mathbf{K}_{t-1}^{-1} \mathbf{K}_t) + (\mathbf{m}_t - \mathbf{m}_{t-1})^\top \mathbf{K}_{t-1}^{-1} (\mathbf{m}_t - \mathbf{m}_{t-1})] + c, \end{aligned} \quad (8)$$

where c is a constant that does not depend on $\boldsymbol{\mu}$ or $\boldsymbol{\Sigma}$. This integral is an approximation for reasons discussed in Appendix D. Despite this, as we will see shortly, our method results in a reasonable function regularisation similar to Equation 1. Replacing the last term in Equation 7 by the

regulariser in Equation 8, we get a new objective function,

$$\mathbb{E}_{q(\mathbf{w})} \left[\frac{N}{\tau} \bar{\ell}_t(\mathbf{w}) + \log q(\mathbf{w}) \right] - \mathbb{E}_{\tilde{q}_{\mathbf{w}_t}(\mathbf{f})} [\log \tilde{q}_{\mathbf{w}_{t-1}}(\mathbf{f})]. \quad (9)$$

Our goal is to find the parameters $\{\boldsymbol{\mu}, \boldsymbol{\Sigma}\}$ of $q(\mathbf{w})$ by minimising the above objective.

Optimising $\boldsymbol{\mu}$ and $\boldsymbol{\Sigma}$ can be very expensive for large networks. We make five approximations to reduce the cost, discussed in detail in Appendix B. First, for the functional prior, we use the mean of $q_{t-1}(\mathbf{w})$, instead of a sample \mathbf{w}_{t-1} , which corresponds to using the GP posterior with a Laplace approximation as given in Equation 5. Second, while computing the derivative of Equation 8, we ignore the derivative with respect to \mathbf{K}_t and only focus on \mathbf{m}_t . Third, instead of using the full \mathbf{K}_{t-1} , we factorise it across tasks, i.e., we approximate it by a block-diagonal matrix containing the kernel matrix $\mathbf{K}_{t-1,s}$ for all past tasks s as the diagonal. This makes the cost of inversion linear in the number of tasks.

Fourth, following [Khan et al. \(2019\)](#), we propose to use a deterministic optimiser to optimise Equation 9 which corresponds to setting the sample $\mathbf{w}_t = \boldsymbol{\mu}$. Finally, we use a diagonal $\boldsymbol{\Sigma}$, which corresponds to a mean-field approximation, reducing the cost of inversion. With these approximations, as shown in Appendix B, the resulting algorithm minimises the following objective:

$$\min_{\mathbf{w}} N \bar{\ell}_t(\mathbf{w}) + \tau \sum_{s=1}^{t-1} (\mathbf{m}_{t,s} - \mathbf{m}_{t-1,s})^\top \mathbf{K}_{t-1,s}^{-1} (\mathbf{m}_{t,s} - \mathbf{m}_{t-1,s}), \quad (10)$$

where $\mathbf{m}_{t,s}$ is the sub-vector of \mathbf{m}_t corresponding to the task s . The above is an approximation of Equation 9 and is computationally cheaper to optimise. To further reduce the implementation issues, we simply use Adam to optimise the above objective. Once the training is finished, we compute the covariance with a full pass over \mathcal{D}_t . This combination is convenient to implement since it relies on Adam.

Despite all the approximations, the objective is still an improved version of the method of [Benjamin et al. \(2018\)](#) shown in Equation 1. Note that, for regression, the mean $\mathbf{m}_{t,s}$ in Equation 10 is equal to the vector $\mathbf{f}_{t,s}$ used in Equation 1. Our functional regulariser additionally includes a kernel matrix $\mathbf{K}_{t-1,s}$ to take care of the uncertainty and weighting of past tasks' memorable examples. Due to this property, we expect our method to perform better.

We can expect further improvements by relaxing these assumptions. For example, we can use a full kernel matrix, use a variational approximation, or employ a block-diagonal covariance matrix. We leave such comparisons as future work since they require sophisticated implementation to scale to large problems.

3.4. The final algorithm

The resulting algorithm, FROMP, is shown in Algorithm 1 for binary classification. Appendix C extends to multiclass classification. For binary classification, the network output $f_w(\mathbf{x})$ is a scalar. We pass it through a sigmoid function $\sigma(f_w(\mathbf{x}))$ to get the probability of class 1. The loss is assumed to be cross-entropy. As shown in Appendix A.2, the Jacobian (of size $1 \times P$) and noise precision (a scalar) are given by the following expressions:

$$\mathbf{J}_w(\mathbf{x}) = \nabla_w f_w(\mathbf{x})^\top, \quad (11)$$

$$\Lambda_w(\mathbf{x}) = \sigma(f_w(\mathbf{x})) [1 - \sigma(f_w(\mathbf{x}))]. \quad (12)$$

Note that $\Lambda(\mathbf{x})$ only depends on the input \mathbf{x} and not on y . To compute the mean and kernel, we need to compute the covariance, which we assume to be diagonal. Ideally this should be obtained using the second derivative of Equation 10, but since this is expensive we use Equation 4 instead. Denoting the diagonal of Σ by \mathbf{v} , we have:

$$\mathbf{v}_t = \mathbf{1} / \left[\delta \mathbf{1} + \sum_{i \in \mathcal{D}_t} \Lambda_{w_t}(\mathbf{x}_i) [\mathbf{J}_{w_t}(\mathbf{x}_i) \circ \mathbf{J}_{w_t}(\mathbf{x}_i)]^\top \right], \quad (13)$$

where \circ and $'$ denote element-wise multiplication and division respectively, and $\mathbf{1}$ is a vector of ones. Using this in an expression similar to Equation 5, we can compute the mean and kernel matrix (see Appendix A.2 for details):

$$\mathbf{m}_{t,s}[i] = \sigma(f_{w_t}(\mathbf{x}_i)), \quad (14)$$

$$\mathbf{K}_{t,s}[i, j] = \Lambda_{w_t}(\mathbf{x}_i) \left[\mathbf{J}_{w_t}(\mathbf{x}_i) (\mathbf{v}_t \circ \mathbf{J}_{w_t}(\mathbf{x}_j))^\top \right] \Lambda_{w_t}(\mathbf{x}_j),$$

calculated over all memorable past examples \mathbf{x}_i and \mathbf{x}_j . Using these expressions, we can write the gradient of the objective 10 at \mathbf{w}_t . Since we ignore the gradient with respect to \mathbf{K}_t , we get a simple expression where an additional term is added to the gradient of the loss:

$$N \nabla_{w_t} \bar{\ell}_t(\mathbf{w}_t) + \tau \sum_{s=1}^{t-1} (\nabla_{w_t} \mathbf{m}_{t,s}) \mathbf{K}_{t-1,s}^{-1} (\mathbf{m}_{t,s} - \mathbf{m}_{t-1,s}), \quad (15)$$

where

$$\nabla_{w_t} \mathbf{m}_{t,s}[i] = \nabla_{w_t} [\sigma(f_{w_t}(\mathbf{x}_i))] = \Lambda_{w_t}(\mathbf{x}_i) \mathbf{J}_{w_t}(\mathbf{x}_i)^\top. \quad (16)$$

This term is computed using the subroutine called `fr_grad` in Algorithm 1.

3.5. Computation complexity

The additional computations on top of Adam is highlighted in red in Algorithm 1. Every iteration requires functional gradients (in `fr_grad`) whose cost is dominated by the

Algorithm 1 FROMP for binary classification on task t given previous mean μ_{t-1} and variance \mathbf{v}_{t-1} of \mathbf{w} , and memorable pasts $\mathcal{M}_{1:t-1}$. The parts responsible for additional computations on top of Adam are highlighted in red.

Function FROMP ($\mathcal{D}_t, \mu_{t-1}, \mathbf{v}_{t-1}, \mathcal{M}_{1:t-1}$) :

```

for previous task  $s = 1, 2, \dots, t-1$  do
    | Compute  $\mathbf{m}_{t-1,s}, \mathbf{K}_{t-1,s}^{-1} \forall \mathbf{x}_i \in \mathcal{M}_s$  using Eq. 14
end
Initialise  $\mathbf{w} \leftarrow \mu_{t-1}$ 
while not converged do
    | Choose minibatch of  $B$  examples  $\{\mathbf{x}_i, y_i\} \in \mathcal{D}_t$ 
    |  $\mathbf{g} \leftarrow (N/B) \nabla_w \ell(y_i, f_w(\mathbf{x}_i))$ 
    |  $\mathbf{g}_f \leftarrow \text{fr\_grad}(\mathbf{w}, \mathbf{m}_{t-1,1:t-1}, \mathbf{K}_{t-1,1:t-1}^{-1}, \mathcal{M}_{1:t-1})$ 
    | Adam update for  $\mathbf{w}$  using the gradient  $\mathbf{g} + \tau \mathbf{g}_f$ 
end
 $\mu_t \leftarrow \mathbf{w}$ 
Compute  $\mathbf{v}_t$  using Eq. 13
 $\mathcal{M}_t \leftarrow \text{memorable\_past}(\mathcal{D}_t, \mathbf{w})$ 
return  $\mu_t, \mathbf{v}_t, \mathcal{M}_t$ 

```

Function fr_grad ($\mathbf{w}_t, \mathbf{m}_{t-1,1:t-1}, \mathbf{K}_{t-1,1:t-1}^{-1}, \mathcal{M}_{1:t-1}$) :

```

Initialise  $\mathbf{g}_f \leftarrow \mathbf{0}$ 
for task  $s = 1, 2, \dots, t-1$  do
    | Compute  $\mathbf{m}_{t,s}$  using Eq. 14 at all  $\mathbf{x}_i \in \mathcal{M}_s$ 
    | Compute  $\mathbf{h}_i \leftarrow \Lambda_{w_t}(\mathbf{x}_i) \mathbf{J}_{w_t}(\mathbf{x}_i)^\top, \forall \mathbf{x}_i \in \mathcal{M}_s$ 
    | Form matrix  $\mathbf{H}$  with  $\mathbf{h}_i$  as columns
    |  $\mathbf{g}_f \leftarrow \mathbf{g}_f + \mathbf{H} \mathbf{K}_{t-1,s}^{-1} (\mathbf{m}_{t,s} - \mathbf{m}_{t-1,s})$ 
end
return  $\mathbf{g}_f$ 

```

Function memorable_past ($\mathcal{D}_t, \mathbf{w}_t$) :

```

Calculate  $\Lambda_{w_t}(\mathbf{x}_i), \forall \mathbf{x}_i \in \mathcal{D}_t$ .
return  $M$  examples with highest  $\Lambda_{w_t}(\mathbf{x}_i)$ .

```

computation of $\mathbf{J}_w(\mathbf{x}_i)$ at all $\mathbf{x}_i \in \mathcal{M}_s, \forall s < t$. Assuming the size of the memorable past is M per task, this adds an additional $O(MPt)$ computation, where P is the number of parameters and t is the task number. This increases only linearly with the size of the memorable past.

We need two additional computations which are required only *once per task*. First, inversion of $\mathbf{K}_s, \forall s < t$, which has cost $O(M^3t)$. This is linear in number of tasks and is feasible when M is not too large. Second, computation of \mathbf{v}_t in Equation 13 requires a full pass through the dataset \mathcal{D}_t , with cost $O(NP)$ where N is the dataset size. This cost can be reduced by estimating \mathbf{v}_t using a minibatch of data (as is common for EWC (Kirkpatrick et al., 2017)).

4. Experiments

To identify the individual benefits of the functional prior (step A) and the selection of memorable past (step B), we compare FROMP to the following three methods:

Table 1. FROMP shows state-of-the-art results on Permuted MNIST (10 tasks) and Split MNIST. “200 points” denotes that 200 examples are selected for each task. We report mean and standard deviations over 5 runs, and use results from [Nguyen et al. \(2018\)](#) for baselines.

Method	Permuted MNIST	Split MNIST
DLP (Smola et al., 2003)	82%	61.2%
EWC (Kirkpatrick et al., 2017)	84%	63.1%
SI (Zenke et al., 2017)	86%	98.9%
Improved VCL (Swaroop et al., 2019)	$93\% \pm 1$	$98.4\% \pm 0.4$
+ random Coreset	$94.6\% \pm 0.3$ (200 points)	$98.2\% \pm 0.4$ (40 points)
FRCL-RND (Titsias et al., 2019)	$94.2\% \pm 0.1$ (200 points)	$96.7\% \pm 1.0$ (40 points)
FRCL-TR (Titsias et al., 2019)	$94.3\% \pm 0.1$ (200 points)	$97.4\% \pm 0.6$ (40 points)
FRORP- L_2	$87.9\% \pm 0.7$ (200 points)	$98.5\% \pm 0.2$ (40 points)
FROMP- L_2	$94.6\% \pm 0.1$ (200 points)	$98.7\% \pm 0.1$ (40 points)
FRORP	$94.6\% \pm 0.1$ (200 points)	$99.0\% \pm 0.1$ (40 points)
FROMP	$94.9\% \pm 0.1$ (200 points)	$99.0\% \pm 0.1$ (40 points)

(I) FROMP- L_2 : Same as FROMP, but replace the kernel in Equation 5 by the identity matrix (similar to Equation 1).

(II) FRORP: Same as FROMP, but memorable examples selected randomly (“R” stands for random).

(III) FRORP- L_2 : Same as FRORP, but replace the kernel in Equation 5 by the identity matrix.

We present comparisons on the following four benchmarks: a toy dataset, permuted MNIST, Split MNIST, and Split CIFAR (a split version of CIFAR-10 & CIFAR-100). In all experiments, we use the Adam optimiser ([Kingma & Ba, 2015](#)). Please see Appendix F for hyperparameter settings.

4.1. Toy dataset

We use a 2D binary classification toy dataset shown in Figure 2 to (i) demonstrate the brittleness and inconsistent behaviour of weight-regularisation, (ii) test FROMP’s performance when exposed to different toy datasets of varying difficulty. We find that weight-regularisation methods such as VCL perform much worse than functional-regularisation (VCL achieves $92\% \pm 10$ while FROMP achieves $99.6\% \pm 0.2$). Results are summarised in Table 2 and visualised in Appendix G.1. In contrast, FROMP performs extremely well across many dataset variations, showing consistently good results (see Table 3 for results and Appendix G.2 for visualisations). For all these experiments, we use a 2-hidden layer single-head MLP with 20 hidden units in each layer. Other details regarding hyperparameter settings is given in Appendix G.3.

4.2. Permuted and Split MNIST

Permuted MNIST consists of a series of tasks, with each applying a fixed permutation of pixels to the entire MNIST dataset. Similarly to previous work ([Kirkpatrick et al., 2017](#); [Zenke et al., 2017](#); [Nguyen et al., 2018](#); [Titsias et al., 2019](#)),

we use a fully connected single-head network with two hidden layers, each consisting of 100 hidden units. We train for 10 tasks. The number of memorable examples is set in the range 10–200.

We also test on the Split MNIST benchmark ([Zenke et al., 2017](#)). This consists of five binary classification tasks built from MNIST: 0/1, 2/3, 4/5, 6/7, and 8/9. Following the settings of previous work, we use a fully connected multi-head network with two hidden layers, each with 256 hidden units. We select 40 memorable points per task. We also run FROMP on a smaller network architecture ([Swaroop et al., 2019](#)), obtaining $99.2\% \pm 0.1$ (see Appendix F.2).

The final average accuracy is shown in Table 1 where FROMP achieves better performance than weight-regularisation methods (EWC, VCL, SI) as well as a function-regularisation method called FRCL. FROMP also improves over FRORP- L_2 and FROMP- L_2 which demonstrates the effectiveness of the kernel. The improvement compared to FRORP is not significant, however, as shown in Figure 3, we do see an improvement when the number of memorable examples are small. We believe this is because performance is already close to the maximum achievable on MNIST benchmarks with many memorable examples.

Figures 4a and 4b show the most and least memorable examples chosen by sorting $\Lambda_w(\mathbf{x}, y)$ (see Section 3.2). The most memorable examples appear to be more difficult to classify than the least memorable examples, which implies that they may lie closer to the decision boundary. This is similar to the illustrative example shown in Figure 2.

4.3. Split CIFAR

Split CIFAR is a more complex benchmark than the MNIST benchmarks, and consists of 6 tasks. The first task is the full CIFAR-10 dataset, followed by 5 tasks, each consisting of 10 consecutive classes from CIFAR-100. We use the same

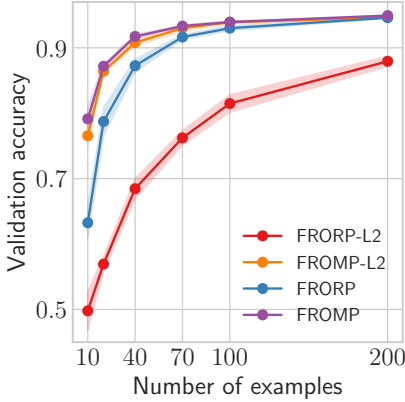


Figure 3. Permuted MNIST: average accuracy over tasks vs the number of memorable past examples. FRORP uses random selection to choose memorable examples, which does not work well when the number of memorable examples is small. In such cases, a careful selection in FROMP gives better results. FRORP-L2, which does not use a kernel (similar to Equation 1), performs even worse. This shows that the kernel plays an important role as well.

model architecture as Zenke et al. (2017), consisting of a multi-head CNN with 4 convolutional layers, then 2 dense layers with dropout. The number of memorable examples is set in the range 10–200. Hyperparameter values are in Appendix F.

We compare to two other additional baselines. The first baseline consists of networks trained on each task separately. Such training cannot profit from forward/backward transfer from other tasks, and we would want our performance to be better than this (a lower limit). The second baseline consists of network trained on all tasks jointly. Ideally, we would like to match this performance, and therefore it can be used as an upper limit for our performance.

The results are summarised in Figure 5a, where we see that FROMP outperforms other continual learning methods by a large margin. The weight-regularisation methods either do not learn later tasks to a high accuracy (EWC, SI), or forget previous tasks (VCL). FROMP also outperforms networks trained separately on each task (see the last column for ‘average’ performance), and achieves performance close to the network trained on all tasks (a margin of less than 2%). In fact, on tasks 4-6, FROMP matches the performance to the network trained on all tasks, which means that FROMP completely avoids catastrophic forgetting on them.

Methods such as VCL+coresets perform rather poorly, which is likely because Bayes By Backprop (Blundell et al., 2015) is difficult to train on CNNs (Osawa et al., 2019; Shridhar et al., 2019). Previous results by Nguyen et al. (2018) and Swaroop et al. (2019) were obtained using multi-layer perceptrons.

Figure 5b shows the accuracy as a function of the number of memorable past examples. Similar to Figure 4a, carefully selecting memorable points and using the kernel improves the performance, especially when the number of memorable examples is small. If we only memorise a few examples (10 per task), using the kernel increases the average accuracy from 65% to 69% (FROMP vs FROMP-L2). The selection of memorable points according to our metric increases the average accuracy from 62% to 69% (FROMP vs FRORP). Applying both kernel and memorable point selection leads to an increase from 58% to 69% (FROMP vs FRORP-L2).

Backward and forward transfer. In continual learning, backward transfer (increased accuracy on previous tasks after seeing new tasks) and forward transfer (increased accuracy on new tasks using information from previous tasks) are important and desirable phenomena. We report metrics for both of these (exact expressions given in Appendix E). BWT (BackWard Transfer) (Lopez-Paz & Ranzato, 2017) is defined as the difference in accuracy between when a task is first trained, and its accuracy after training on the final task, averaged over all tasks (higher is better). A lower value indicates that the model has decreased performance on previous tasks after training on new tasks (large negative backward transfer is known as catastrophic forgetting). We find that FROMP has a score of -2.6 ± 0.9 , which is the best score with EWC’s score of -2.3 ± 1.4 . VCL+coresets performs poorly with a score of -9.2 ± 1.8 . Although EWC performs well in backward transfer, it does so at the cost of forward transfer and overall accuracy.

We define a forward transfer metric as the average improvement in accuracy on a new task over an independently trained model on that task (higher is better). See Appendix E for an exact expression. A higher value indicates that the model used more information from previous tasks to obtain better performance on a new task (this information is not available to the model trained independently on tasks). FROMP achieves a forward transfer of 6.1 ± 0.7 , whereas EWC has 0.17 ± 0.9 and VCL+coresets has 1.8 ± 3.1 . Although we only focussed on preventing catastrophic forgetting, we find evidence of forward transfer, a key requirement in continual learning. Overall, given final average accuracy, backward transfer and forward transfer, FROMP clearly outperforms the other baselines.

5. Discussion

We propose FROMP, a scalable function-regularisation approach for continual learning. FROMP uses a Gaussian Process formulation of neural networks to convert weight-space distributions into function-space, select memorable past examples, and then regularise the function at those points. It achieves state-of-the-art performance across benchmarks. This work enables a new way of combining regularisation

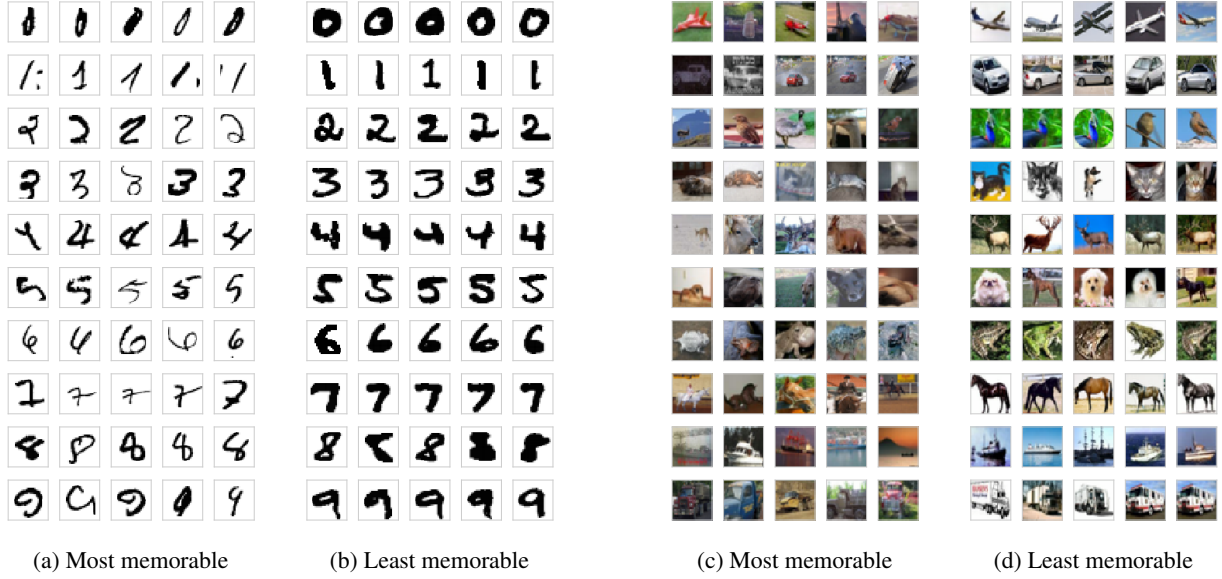


Figure 4. Most and least memorable examples for MNIST (left) and CIFAR-10. The most memorable examples appear to be more difficult to classify than the least memorable examples, which implies that they may lie closer to the decision boundary (similar to Figure 2).

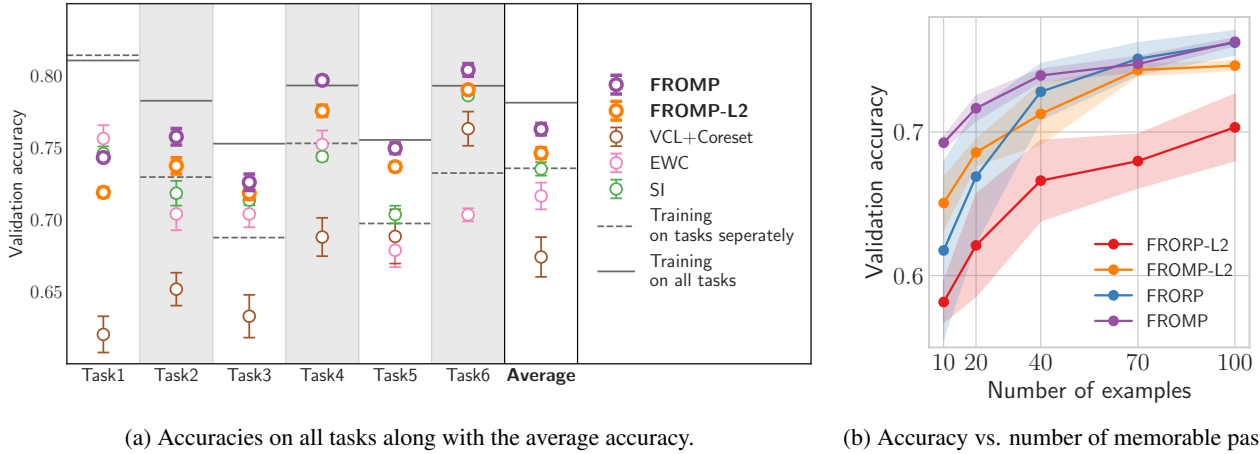


Figure 5. (Left) FROMP shows state-of-the-art performance on Split CIFAR. Columns show the performance on each task after training on the final task, and the last column shows the average accuracy over tasks (mean and standard deviation over 5 runs). We use 200 memorable examples. See Appendix F.3 for numerical values. FROMP’s performance is close to that of the network trained on all tasks jointly. In fact, on tasks 4-6, it matches the performance and demonstrates no forgetting at all. (Right) Similar to Figure 3, this figure demonstrates the effectiveness of using a kernel and carefully selecting memorable examples. When the number of memorable examples is low, FROMP gives better accuracy than other methods that either use a random set of memorable examples or do not employ a kernel.

methods and memory-based methods in continual learning. Future research could investigate other ways of selecting a memorable past (e.g. fixed memory size), combining with model-based continual learning approaches, and the setting where there are no task boundaries.

Acknowledgements

We would like to thank Prof Yi Yang (The ReLER Lab, University of Technology, Sydney) for helpful discussions. We are also thankful for the RAIDEN computing system and its support team at the RIKEN Center for AI Project which we used extensively for our experiments.

References

- Alaoui, A. and Mahoney, M. W. Fast randomized kernel ridge regression with statistical guarantees. In *Advances in Neural Information Processing Systems*, pp. 775–783, 2015.
- Aljundi, R., Lin, M., Goujaud, B., and Bengio, Y. Gradient based sample selection for online continual learning. *ArXiv*, abs/1903.08671, 2019.
- Benjamin, A. S., Rolnick, D., and Kording, K. Measuring and regularizing networks in function space. *arXiv preprint arXiv:1805.08289*, 2018.
- Bishop, C. M. *Pattern recognition and machine learning*. Springer, 2006.
- Blundell, C., Cornebise, J., Kavukcuoglu, K., and Wierstra, D. Weight uncertainty in neural networks. *ICML*, 2015.
- Bottou, L. Large-scale machine learning with stochastic gradient descent. In *Proceedings of COMPSTAT’2010*, pp. 177–186. Springer, 2010.
- Chaudhry, A., Ranzato, M., Rohrbach, M., and Elhoseiny, M. Efficient lifelong learning with A-GEM. *ArXiv*, abs/1812.00420, 2018.
- Chaudhry, A., Rohrbach, M., Elhoseiny, M., Ajanthan, T., Dokania, P. K., Torr, P. H. S., and Ranzato, M. On tiny episodic memories in continual learning. *ArXiv*, abs/1902.10486, 2019.
- Ebrahimi, S., Elhoseiny, M., and Trevor Darrell, M. R. Uncertainty-guided continual learning with Bayesian neural networks. *ArXiv*, abs/1906.02425, 2019.
- Jacot, A., Gabriel, F., and Hongler, C. Neural tangent kernel: Convergence and generalization in neural networks. In *Advances in neural information processing systems*, pp. 8571–8580, 2018.
- Khan, M., Nielsen, D., Tangkaratt, V., Lin, W., Gal, Y., and Srivastava, A. Fast and scalable Bayesian deep learning by weight-perturbation in Adam. In *ICML*, pp. 2611–2620. PMLR. org, 2018.
- Khan, M. E., Immer, A., Abedi, E., and Korzepa, M. Approximate inference turns deep networks into Gaussian processes. *Advances in neural information processing systems*, 2019.
- Kingma, D. P. and Ba, J. Adam: A method for stochastic optimization. *ICLR*, 2015.
- Kirkpatrick, J., Pascanu, R., Rabinowitz, N., Veness, J., Desjardins, G., Rusu, A. A., Milan, K., Quan, J., Ramalho, T., Grabska-Barwinska, A., et al. Overcoming catastrophic forgetting in neural networks. *Proceedings of the national academy of sciences*, 114(13):3521–3526, 2017.
- Lopez-Paz, D. and Ranzato, M. Gradient episodic memory for continual learning. In *Advances in Neural Information Processing Systems*, pp. 6467–6476, 2017.
- Ma, P., Mahoney, M. W., and Yu, B. A statistical perspective on algorithmic leveraging. *Journal of Machine Learning Research*, 16(27):861–911, 2015. URL <http://jmlr.org/papers/v16/ma15a.html>.
- Nguyen, C. V., Li, Y., Bui, T. D., and Turner, R. E. Variational continual learning. *ICLR*, 2018.
- Osawa, K., Swaroop, S., Khan, M. E. E., Jain, A., Eschenhagen, R., Turner, R. E., and Yokota, R. Practical deep learning with Bayesian principles. *Advances in neural information processing systems*, 2019.
- Rasmussen, C. and Williams, C. *Gaussian Processes for Machine Learning*. Adaptive Computation and Machine Learning. MIT Press, Cambridge, MA, USA, January 2006.
- Rebuffi, S.-A., Kolesnikov, A., Sperl, G., and Lampert, C. H. icarl: Incremental classifier and representation learning. In *Proceedings of the IEEE conference on Computer Vision and Pattern Recognition*, pp. 2001–2010, 2017.
- Ritter, H., Botev, A., and Barber, D. Online structured laplace approximations for overcoming catastrophic forgetting. In *Advances in Neural Information Processing Systems*, pp. 3738–3748, 2018.
- Serra, J., Suris, D., Miron, M., and Karatzoglou, A. Overcoming catastrophic forgetting with hard attention to the task. In *ICML*, pp. 4548–4557. PMLR. org, 2018.
- Shin, H., Lee, J. K., Kim, J., and Kim, J. Continual learning with deep generative replay. In *Advances in neural information processing systems*, 2017.
- Shridhar, K., Laumann, F., and Liwicki, M. A comprehensive guide to Bayesian convolutional neural network with variational inference. *ArXiv*, abs/1901.02731, 2019.
- Smola, A. J., Vishwanathan, V., and Eskin, E. Laplace propagation. In *Advances in neural information processing systems*, pp. 441–448, 2003.
- Swaroop, S., Nguyen, C. V., Bui, T. D., and Turner, R. E. Improving and understanding variational continual learning. *arXiv preprint arXiv:1905.02099*, 2019.
- Titsias, M. K., Schwarz, J., Matthews, A. G. d. G., Pascanu, R., and Teh, Y. W. Functional regularisation for continual learning using Gaussian processes. *arXiv preprint arXiv:1901.11356*, 2019.

Train, K. E. *Discrete choice methods with simulation*. Cambridge university press, 2009.

Zenke, F., Poole, B., and Ganguli, S. Continual learning through synaptic intelligence. In *ICML*, pp. 3987–3995. JMLR. org, 2017.

A. Deep Networks to Functional Priors with DNN2GP

A.1. GP posteriors from the Minimiser of Linear Model

The posterior distribution of a linear model induces a GP posterior as shown by [Rasmussen & Williams \(2006\)](#). We discuss this in detail now for the following linear model discussed in Section 3.1:

$$y_i = f_w(\mathbf{x}_i) + \epsilon_i, \text{ where } f_w(\mathbf{x}_i) := \boldsymbol{\phi}(\mathbf{x}_i)^\top \mathbf{w}, \quad \epsilon_i \sim \mathcal{N}(\epsilon_i | 0, \Lambda^{-1}), \quad \text{and } \mathbf{w} \sim \mathcal{N}(\mathbf{w} | 0, \delta^{-1} \mathbf{I}_P) \quad (17)$$

with a feature map $\boldsymbol{\phi}(\mathbf{x})$. [Rasmussen & Williams \(2006\)](#) show that the predictive distribution for a test input \mathbf{x} takes the following form (see Equation 2.11 in their book):

$$p(f(\mathbf{x}) | \mathbf{x}, \mathcal{D}) = \mathcal{N}(f(\mathbf{x}) | \Lambda \boldsymbol{\phi}(\mathbf{x})^\top \mathbf{A}^{-1} \boldsymbol{\Phi} \mathbf{y}, \boldsymbol{\phi}(\mathbf{x})^\top \mathbf{A}^{-1} \boldsymbol{\phi}(\mathbf{x})), \quad \text{where } \mathbf{A} := \sum_i \boldsymbol{\phi}(\mathbf{x}_i) \Lambda \boldsymbol{\phi}(\mathbf{x}_i)^\top + \delta \mathbf{I}_P. \quad (18)$$

where \mathcal{D} is set of training points $\{y_i, \mathbf{x}_i\}$ for i , and $\boldsymbol{\Phi}$ is a matrix with $\boldsymbol{\phi}(\mathbf{x}_i)$ as columns.

[Rasmussen & Williams \(2006\)](#) derive the above predictive distribution by using the weight-space posterior $\mathcal{N}(\mathbf{w} | \mathbf{w}_{\text{lin}}, \boldsymbol{\Sigma}_{\text{lin}})$ with the mean and covariance defined as below:

$$\mathbf{w}_{\text{lin}} := \Lambda \mathbf{A}^{-1} \boldsymbol{\Phi} \mathbf{y}, \quad \boldsymbol{\Sigma}_{\text{lin}} := \mathbf{A}^{-1}. \quad (19)$$

The mean \mathbf{w}_{lin} is also the minimiser of the least-squares loss and \mathbf{A} is the hessian at that solution.

[Rasmussen & Williams \(2006\)](#) show that the predictive distribution in Equation 18 corresponds to a GP posterior with the following mean and covariance functions:

$$m_{\text{lin}}(\mathbf{x}) = \Lambda \boldsymbol{\phi}(\mathbf{x})^\top \mathbf{A}^{-1} \boldsymbol{\Phi} \mathbf{y} = \boldsymbol{\phi}(\mathbf{x})^\top \mathbf{w}_{\text{lin}} = f_{\mathbf{w}_{\text{lin}}}(\mathbf{x}), \quad (20)$$

$$\kappa_{\text{lin}}(\mathbf{x}, \mathbf{x}') := \boldsymbol{\phi}(\mathbf{x})^\top \boldsymbol{\Sigma}_{\text{lin}} \boldsymbol{\phi}(\mathbf{x}'), \quad (21)$$

This is the result shown in Equation 2 in Section 3.1. We can also write the predictive distribution of the observation $y = f(\mathbf{x}) + \epsilon$ where $\epsilon \sim \mathcal{N}(0, \Lambda^{-1})$ as follows:

$$p(y | \mathbf{x}, \mathcal{D}) = \mathcal{N}(y | \underbrace{f_{\mathbf{w}_{\text{lin}}}(\mathbf{x})}_{m_{\text{lin}}(\mathbf{x})}, \underbrace{\boldsymbol{\phi}(\mathbf{x})^\top \boldsymbol{\Sigma}_{\text{lin}} \boldsymbol{\phi}(\mathbf{x}) + \Lambda^{-1}}_{\kappa_{\text{lin}}(\mathbf{x}, \mathbf{x})}), \quad \text{where } \boldsymbol{\Sigma}_{\text{lin}}^{-1} := \sum_i \boldsymbol{\phi}(\mathbf{x}_i) \Lambda \boldsymbol{\phi}(\mathbf{x}_i)^\top + \delta \mathbf{I}_P. \quad (22)$$

We will make use of Equations 20, 21 and 22 to write the mean and covariance function of the posterior approximation for neural networks, as shown in the next section.

A.2. GP Posteriors from the Minimiser of Neural Networks

[Khan et al. \(2019\)](#) derive GP predictive distributions for the minimisers of a variety of loss functions in Appendix B of their paper. We describe these below along with the resulting GP posteriors. Throughout, we denote a minimiser of the loss by \mathbf{w}_* .

A regression loss: For a regression loss function $\ell(y, f) := \frac{1}{2} \Lambda (y - f)^2$, they derive the following expression for the predictive distribution for the observations y (see Equation 44, Appendix B.2 in their paper):

$$\hat{p}(y | \mathbf{x}, \mathcal{D}) := \mathcal{N}(y | f_{\mathbf{w}_*}(\mathbf{x}), \mathbf{J}_{\mathbf{w}_*}(\mathbf{x}) \boldsymbol{\Sigma}_* \mathbf{J}_{\mathbf{w}_*}(\mathbf{x})^\top + \Lambda^{-1}), \quad \text{where } \boldsymbol{\Sigma}_*^{-1} := \sum_i \mathbf{J}_{\mathbf{w}_*}(\mathbf{x}_i)^\top \Lambda \mathbf{J}_{\mathbf{w}_*}(\mathbf{x}_i) + \delta \mathbf{I}_P. \quad (23)$$

We use $\hat{p}(y | \mathbf{x}, \mathcal{D})$ since this predictive distribution is not exact and is obtained using a type of Laplace approximation. Comparing this to Equation 22, we can write the mean and covariance functions in a similar fashion as Equation 20-21:

$$m_{\mathbf{w}_*}(\mathbf{x}) := f_{\mathbf{w}_*}(\mathbf{x}), \quad \kappa_{\mathbf{w}_*}(\mathbf{x}, \mathbf{x}') := \mathbf{J}_{\mathbf{w}_*}(\mathbf{x}) \boldsymbol{\Sigma}_* \mathbf{J}_{\mathbf{w}_*}(\mathbf{x}')^\top. \quad (24)$$

This is the result shown in Equation 5 in Section 3.1.

A binary classification loss: A similar expression is available for binary classification with $y \in \{0, 1\}$, considering the loss $\ell(y, f) := -y \log \sigma(f) - (1 - y) \log(1 - \sigma(f)) = -yf + \log(1 + e^f)$ where $\sigma(f) := 1/(1 + e^{-f})$ is the sigmoid function. See Equation 48, Appendix B.2 in [Khan et al. \(2019\)](#). The predictive distribution is given as follows:

$$\hat{p}(y|\mathbf{x}, \mathcal{D}) := \mathcal{N}(y | \sigma(f_{w_*}(\mathbf{x})), \Lambda_{w_*}(\mathbf{x}) \mathbf{J}_{w_*}(\mathbf{x}) \Sigma_* \mathbf{J}_{w_*}(\mathbf{x})^\top \Lambda_{w_*}(\mathbf{x}) + \Lambda_{w_*}(\mathbf{x})), \quad (25)$$

$$\text{where } \Sigma_*^{-1} := \sum_i \mathbf{J}_{w_*}(\mathbf{x}_i)^\top \Lambda_{w_*}(\mathbf{x}_i) \mathbf{J}_{w_*}(\mathbf{x}_i) + \delta \mathbf{I}_P. \quad (26)$$

where $\Lambda_{w_*}(\mathbf{x}) := \sigma(f_{w_*}(\mathbf{x})) [1 - \sigma(f_{w_*}(\mathbf{x}))]$. The predictive distribution does not respect the fact that y is binary and treats it like a Gaussian. This makes it comparable to Equation 22. Comparing the two, we can conclude that the above corresponds to the predictive posterior distribution of a GP regression model with $y = f(\mathbf{x}) + \epsilon$ where $\epsilon \sim \mathcal{N}(0, \Lambda_{w_*}(\mathbf{x}))$ with the mean and covariance function as shown below:

$$m_{w_*}(\mathbf{x}) := \sigma(f_{w_*}(\mathbf{x})), \quad \kappa_{w_*}(\mathbf{x}, \mathbf{x}') := \Lambda_{w_*}(\mathbf{x}) \mathbf{J}_{w_*}(\mathbf{x}) \Sigma_* \mathbf{J}_{w_*}(\mathbf{x}')^\top \Lambda_{w_*}(\mathbf{x}'). \quad (27)$$

This is the result used in Equation 14 in Section 3.4 for binary classification. A difference here is that the mean function is passed through the sigmoid function and the covariance function has $\Lambda_{w_*}(\mathbf{x})$ multiplied on the both sides. These changes appear because of the nonlinearity in the loss function introduced due to the sigmoid link function.

A multiclass classification loss: The above result straightforwardly extends to the multiclass classification case by using multinomial-logit likelihood (or softmax function). For this the loss can be written as follows:

$$\ell(\mathbf{y}, \mathbf{f}) = -\mathbf{y}^\top \mathcal{S}(\mathbf{f}) + \log \left(1 + \sum_{k=1}^{K-1} e^{f_k} \right), \text{ where } k\text{'th element of } \mathcal{S}(\mathbf{f}) \text{ is given by } \frac{e^{f_j}}{1 + \sum_{k=1}^{K-1} e^{f_k}} \quad (28)$$

where the number of categories is equal to K , \mathbf{y} is a one-hot-encoding vector of size $K - 1$, \mathbf{f} is $K - 1$ length output of the neural network, and $\mathcal{S}(\mathbf{f})$ is the softmax operation which maps a $K - 1$ length real vector to a $K - 1$ dimensional vector with entries in the open interval $(0, 1)$. The encoding in $K - 1$ length vectors ignores the last category which then ensures identifiability ([Train, 2009](#)). In a similar fashion to the binary case, the predictive distribution of the $K - 1$ length output \mathbf{y} for an input \mathbf{x} can be written as follows:

$$\hat{p}(\mathbf{y}|\mathbf{x}, \mathcal{D}) := \mathcal{N}(\mathbf{y} | \mathcal{S}(\mathbf{f}_{w_*}(\mathbf{x})), \Lambda_{w_*}(\mathbf{x}) \mathbf{J}_{w_*}(\mathbf{x}) \Sigma_* \mathbf{J}_{w_*}(\mathbf{x})^\top \Lambda_{w_*}(\mathbf{x}) + \Lambda_{w_*}(\mathbf{x})), \quad (29)$$

$$\text{where } \Sigma_*^{-1} := \sum_i \mathbf{J}_{w_*}(\mathbf{x}_i)^\top \Lambda_{w_*}(\mathbf{x}_i) \mathbf{J}_{w_*}(\mathbf{x}_i) + \delta \mathbf{I}_P.$$

where $\Lambda_{w_*}(\mathbf{x}) := \mathcal{S}(\mathbf{f}_{w_*}(\mathbf{x})) [1 - \mathcal{S}(\mathbf{f}_{w_*}(\mathbf{x}))]^\top$ is a $(K - 1) \times (K - 1)$ matrix and $\mathbf{J}_{w_*}(\mathbf{x})$ is the $(K - 1) \times P$ Jacobian matrix. The mean function in this case is a $K - 1$ length matrix and the covariance function is a square matrix of size $K - 1$. Their expressions are shown below:

$$\mathbf{m}_{w_*}(\mathbf{x}) := \mathcal{S}(\mathbf{f}_{w_*}(\mathbf{x})), \quad \mathbf{K}_{w_*}(\mathbf{x}, \mathbf{x}') := \Lambda_{w_*}(\mathbf{x}) \mathbf{J}_{w_*}(\mathbf{x}) \Sigma_* \mathbf{J}_{w_*}(\mathbf{x}')^\top \Lambda_{w_*}(\mathbf{x}'). \quad (30)$$

General case: The results above hold for a generic loss function derived from a generalised linear model (GLM) with an invertible function $\mathbf{h}(\mathbf{f})$, e.g., $\ell(\mathbf{y}, \mathbf{f}) := -\log p(\mathbf{y}|\mathbf{h}(\mathbf{f}))$. For example, for a Bernoulli distribution, the link function $h(f)$ is equal to σ . In the GLM literature, \mathbf{h}^{-1} is known as the link function. Given such a loss, the only quantity that changes in the above calculations is $\Lambda_{w_*}(\mathbf{x}, \mathbf{y}) := \nabla_{\mathbf{f}\mathbf{f}}^2 \ell(\mathbf{y}, \mathbf{f})$, which is the second derivative of the loss with respect to \mathbf{f} , and might depend both on \mathbf{x} and \mathbf{y} .

A.3. GP Posterior from the Iterations of a Neural-Network Optimiser

The results of the previous section hold only at a minimiser \mathbf{w}_* . [Khan et al. \(2019\)](#) generalise this to iterations of optimisers. They did this for a variational inference algorithm and also for its deterministic version that resembles RMSprop. We now describe these two versions. We will only consider binary classification using the setup described in the previous section. The results can be easily generalised to multiclass classification.

GP posterior from iterations of a variational inference algorithm: Given a Gaussian variational approximation $q_j(\mathbf{w}) := \mathcal{N}(\mathbf{w}|\mu_j, \Sigma_j)$ at iteration j , [Khan et al. \(2019\)](#) used a natural-gradient variational inference algorithm called the

variational-online Newton (VON) method (Khan et al., 2018). Given a $q_j(\mathbf{w})$, the algorithm proceeds by first sampling $\mathbf{w}_j \sim q_j(\mathbf{w})$, and then updating the variational distribution. Surprisingly, the procedure used to derive a GP predictive distribution for the minimiser generalises to this update too. An expression for the predictive distribution is given below:

$$\hat{p}_{j+1}(y|\mathbf{x}, \mathcal{D}) := \mathcal{N}(y | \sigma(f_{\mathbf{w}_j}(\mathbf{x})), \Lambda_{\mathbf{w}_j}(\mathbf{x}) \mathbf{J}_{\mathbf{w}_j}(\mathbf{x}) \Sigma_j \mathbf{J}_{\mathbf{w}_j}(\mathbf{x})^\top \Lambda_{\mathbf{w}_j}(\mathbf{x}) + \Lambda_{\mathbf{w}_j}(\mathbf{x})^{-1}), \quad (31)$$

$$\text{where } \Sigma_{j+1}^{-1} := (1 - \beta_j) \Sigma_j^{-1} + \beta_j \left[\sum_i \mathbf{J}_{\mathbf{w}_j}(\mathbf{x}_i)^\top \Lambda_{\mathbf{w}_j}(\mathbf{x}_i) \mathbf{J}_{\mathbf{w}_j}(\mathbf{x}_i) + \delta \mathbf{I}_P \right], \quad (32)$$

$$\boldsymbol{\mu}_{j+1} := \boldsymbol{\mu}_j - \beta_j \Sigma_{j+1} \left[N \nabla_{\mathbf{w}} \bar{\ell}(\mathbf{w}_j) + \delta \boldsymbol{\mu}_j \right]. \quad (33)$$

where $\bar{\ell}(\mathbf{w}) := \frac{1}{N} \sum_{i=1}^N \ell(y_i, f_{\mathbf{w}}(\mathbf{x}_i))$. The predictive distribution takes the same form as before, but now the covariance and mean are updated according to the VON updates. The VON updates are essential to ensure the validity of the GP posterior, however, as Khan et al. (2019) discuss, the RMSprop/Adam have similar update which enable us to apply the above results even when running such algorithms. We describe this next.

GP posterior from iterations of RMSprop/Adam: Khan et al. (2019) propose a deterministic version of the above update where \mathbf{w}_j is not sampled from $q_j(\mathbf{w})$ rather is set to be equal to $\boldsymbol{\mu}_j$, i.e., $\mathbf{w}_j = \boldsymbol{\mu}_j$. This gives rise to the following update:

$$\Sigma_{j+1}^{-1} \leftarrow (1 - \beta_j) \Sigma_j^{-1} + \beta_j \left[\sum_i \mathbf{J}_{\mathbf{w}_j}(\mathbf{x}_i)^\top \Lambda_{\mathbf{w}_j}(\mathbf{x}_i) \mathbf{J}_{\mathbf{w}_j}(\mathbf{x}_i) + \delta \mathbf{I}_P \right], \quad (34)$$

$$\mathbf{w}_{j+1} \leftarrow \mathbf{w}_j - \beta_j \Sigma_{j+1} \left[N \nabla_{\mathbf{w}} \bar{\ell}(\mathbf{w}_j) + \delta \mathbf{w}_j \right], \quad (35)$$

with the variational approximation defined as $q_j(\mathbf{w}) := \mathcal{N}(\mathbf{w} | \mathbf{w}_j, \Sigma_j)$. The form of the predictive distribution remains the same as Equation 31.

As discussed in Khan et al. (2018), the above algorithm can be made similar to RMSprop by using a diagonal covariance. By reparameterising the diagonal of Σ^{-1} as $\mathbf{s} + \delta \mathbf{1}$ where \mathbf{s} is an unknown vector, we can rewrite the updates to update $\boldsymbol{\mu}$ and \mathbf{s} . This can then be written in a form similar to RMSprop as shown below:

$$\mathbf{s}_{j+1} \leftarrow (1 - \beta_j) \mathbf{s}_j + \beta_j \left[\sum_i \Lambda_{\mathbf{w}_j}(\mathbf{x}_i) \left[\mathbf{J}_{\mathbf{w}_j}(\mathbf{x}_i) \circ \mathbf{J}_{\mathbf{w}_j}(\mathbf{x}_i) \right]^\top \right] \quad (36)$$

$$\mathbf{w}_{j+1} \leftarrow \mathbf{w}_j - \beta_j \frac{1}{\mathbf{s}_{j+1} + \delta \mathbf{1}} \circ \left[N \nabla_{\mathbf{w}} \bar{\ell}(\mathbf{w}_j) + \delta \mathbf{w}_j \right], \quad (37)$$

where \circ defines element-wise product of two vectors, and the diagonal of Σ_{j+1}^{-1} is equal to $(\mathbf{s}_{j+1} + \delta \mathbf{1})$. This algorithm differs from RMSprop in two ways. First, the scale vector \mathbf{s}_j is updated using the sum of the square of the Jacobians instead of the square of the mini-batch gradients. Second, there is no square-root in the preconditioner for the gradient in the second line. This algorithm is the diagonal version of the Online Generalised Gauss-Newton (OGGN) algorithm discussed in Khan et al. (2019).

In practice, we ignore these two differences and employ the RMSprop/Adam update instead. As a consequence the variance estimates might not be very good during the iteration, even though the fixed-point of the algorithm is not changed (Khan et al., 2018). This is the price we pay for the convenience of using RMSprop/Adam. We correct the approximation after convergence of the algorithm by recomputing the diagonal of the covariance according to Equation 36. Denoting the converged solution by \mathbf{w}_* , we compute the diagonal \mathbf{v}_* of the covariance Σ_* as shown below:

$$\mathbf{v}_* = \mathbf{1} / \left[\delta \mathbf{1} + \sum_{i=1}^N \Lambda_{\mathbf{w}_*}(\mathbf{x}_i) \left[\mathbf{J}_{\mathbf{w}_*}(\mathbf{x}_i) \circ \mathbf{J}_{\mathbf{w}_*}(\mathbf{x}_i) \right]^\top \right], \quad (38)$$

B. Detailed Derivation of FROMP Algorithm

In this section, we provide further details on Section 3.3, explaining the derivation of Equations 15-16 in the main text.

$$\mathcal{L}(q(\mathbf{w})) := \mathbb{E}_{q(\mathbf{w})} \left[\frac{N}{\tau} \bar{\ell}_t(\mathbf{w}) + \log q(\mathbf{w}) \right] - \mathbb{E}_{\tilde{q}_{\mathbf{w}_t}(\mathbf{f})} \left[\log \tilde{q}_{\mathbf{w}_{t-1}}(\mathbf{f}) \right], \text{ where } \mathbf{w}_t \sim q(\mathbf{w}) \text{ and } \mathbf{w}_{t-1} \sim q_{t-1}(\mathbf{w}) \quad (39)$$

Optimising this objective requires us to obtain the GP posterior $\tilde{q}_{w_t}(\mathbf{f})$. This can be easily done applying the DNN2GP result from Equation 31 to this loss function. The VON update for the objective above takes the following form:

$$\Sigma^{-1} \leftarrow (1 - \beta)\Sigma^{-1} + \beta \left[\sum_i \mathbf{J}_{w_t}(\mathbf{x}_i)^\top \Lambda_{w_t}(\mathbf{x}_i) \mathbf{J}_{w_t}(\mathbf{x}_i) - \nabla_{\Sigma} \mathbb{E}_{\tilde{q}_{w_t}(\mathbf{f})} [\log \tilde{q}_{w_{t-1}}(\mathbf{f})] \right], \quad (40)$$

$$\mu \leftarrow \mu - \beta \Sigma \left[\frac{N}{\tau} \nabla_w \bar{\ell}_t(\mathbf{w}_t) + \nabla_{\mu} \mathbb{E}_{\tilde{q}_{w_t}(\mathbf{f})} [\log \tilde{q}_{w_{t-1}}(\mathbf{f})] \right]. \quad (41)$$

where $\bar{\ell}_t(\mathbf{w}) := \frac{1}{N} \sum_{i \in \mathcal{D}_t} \ell(y_i, f_w(\mathbf{x}_i))$ and we have ignored the iteration subscript to simplify notation.

Using the μ and Σ obtained with this iteration, we can define the following GP predictive posterior at a sample $\mathbf{w}_t \sim q(\mathbf{w})$:

$$\hat{p}_t(y|\mathbf{x}, \mathcal{D}) := \mathcal{N}(y | \sigma(f_{w_t}(\mathbf{x})), \Lambda_{w_t}(\mathbf{x}) \mathbf{J}_{w_t}(\mathbf{x}) \Sigma \mathbf{J}_{w_t}(\mathbf{x})^\top \Lambda_{w_t}(\mathbf{x}) + \Lambda_{w_t}(\mathbf{x})^{-1}), \quad (42)$$

Comparing this to Equation 31, we can write the mean and covariance function as follows:

$$m_{w_t}(\mathbf{x}) := \sigma(f_{w_t}(\mathbf{x})), \quad \kappa_{w_t}(\mathbf{x}, \mathbf{x}') := \Lambda_{w_t}(\mathbf{x}) \mathbf{J}_{w_t}(\mathbf{x}) \Sigma \mathbf{J}_{w_t}(\mathbf{x}')^\top \Lambda_{w_t}(\mathbf{x}'). \quad (43)$$

The mean vector obtained by concatenating $m_{w_t}(\mathbf{x})$ at all $\mathbf{x} \in \mathcal{M}$ is denoted by \mathbf{m}_t . Similarly, the covariance matrix \mathbf{K}_t is defined as the matrix with ij 'th entry as $\kappa_{w_t}(\mathbf{x}_i, \mathbf{x}_j)$. The corresponding mean and covariance obtained from samples from $q_{t-1}(\mathbf{w})$ are denoted by \mathbf{m}_{t-1} and \mathbf{K}_{t-1} .

Given these quantities, the functional regularisation term has an analytical expression given as follows:

$$\mathbb{E}_{\tilde{q}_{w_t}(\mathbf{f})} [\log \tilde{q}_{w_{t-1}}(\mathbf{f})] = -\frac{1}{2} [\text{Tr}(\mathbf{K}_{t-1}^{-1} \mathbf{K}_t) + (\mathbf{m}_t - \mathbf{m}_{t-1})^\top \mathbf{K}_{t-1}^{-1} (\mathbf{m}_t - \mathbf{m}_{t-1})] + c, \quad (44)$$

Our goal is to obtain the derivative of this term with respect to μ and Σ . Both \mathbf{m}_t and \mathbf{K}_t are functions of μ and Σ through the sample $\mathbf{w}_t = \mu + \Sigma^{1/2} \epsilon$ where $\epsilon \sim \mathcal{N}(0, \mathbf{I})$. Therefore, we can compute these derivative using the chain rule.

We note that the resulting algorithm is costly for large problems, and propose five approximations to reduce the computation cost, as described below.

Approximation 1: Instead of sampling \mathbf{w}_{t-1} , we set $\mathbf{w}_{t-1} = \mu_{t-1}$ which is the mean of the posterior approximation $q_{t-1}(\mathbf{w})$ until task $t-1$. Therefore, we replace $\mathbb{E}_{\tilde{q}_{w_t}(\mathbf{f})} [\log \tilde{q}_{w_{t-1}}(\mathbf{f})]$ by $\mathbb{E}_{\tilde{q}_{w_t}(\mathbf{f})} [\log \tilde{q}_{\mu_{t-1}}(\mathbf{f})]$. This affects the mean \mathbf{m}_{t-1} and \mathbf{K}_{t-1} in Equation 44.

Approximation 2: When computing the derivation of the functional regulariser, we will ignore the derivative with respect to \mathbf{K}_t and only consider \mathbf{m}_t . Therefore, the derivatives needed for the update in Equation 40-41 can be approximated as follows:

$$\nabla_{\mu} \mathbb{E}_{\tilde{q}_{w_t}(\mathbf{f})} [\log \tilde{q}_{w_{t-1}}(\mathbf{f})] \approx [\nabla_{\mu} \mathbf{m}_t] \mathbf{K}_{t-1}^{-1} (\mathbf{m}_t - \mathbf{m}_{t-1}), \quad (45)$$

$$\nabla_{\Sigma} \mathbb{E}_{\tilde{q}_{w_t}(\mathbf{f})} [\log \tilde{q}_{w_{t-1}}(\mathbf{f})] \approx [\nabla_{\Sigma} \mathbf{m}_t] \mathbf{K}_{t-1}^{-1} (\mathbf{m}_t - \mathbf{m}_{t-1}), \quad (46)$$

This avoids having to calculate complex derivatives (e.g., derivatives of Jacobians).

Approximation 3: Instead of using the full \mathbf{K}_{t-1} , we factorise it across tasks, i.e., we approximate it by a block-diagonal matrix containing the kernel matrix $\mathbf{K}_{t-1,s}$ for all past tasks s as the diagonal. This makes the cost of inversion linear in the number of tasks.

Approximation 4: Similarly to Equation 34-35, we use a deterministic version of the VON update by setting $\mathbf{w}_t = \mu$, which corresponds to setting the random noise ϵ to zero in $\mathbf{w}_t = \mu + \Sigma^{1/2} \epsilon$. This approximation simplifies the gradient computation in Equation 45-46, since now the gradient with respect to Σ is zero. For example, in the binary classification case, $m_{\mu}(\mathbf{x}) := \sigma(f_{\mu}(\mathbf{x}))$, which does not depend on Σ . The gradient of \mathbf{m}_t with respect to μ is given as follows using the chain rule (here $\mathbf{m}_{t,s}$ is the sub-vector of \mathbf{m}_t corresponding to the task s).

$$\nabla_{\mu} \mathbf{m}_{t,s}[i] = \nabla_{\mu} [\sigma(f_{\mu}(\mathbf{x}_i))] = \Lambda_{\mu}(\mathbf{x}_i) \mathbf{J}_{\mu}(\mathbf{x}_i)^\top, \text{ where } \mathbf{x}_i \in \mathcal{M}_s, \quad (47)$$

and where the second equality holds for canonical link functions. With these simplifications, we can write the VON update as follows:

$$\Sigma^{-1} \leftarrow (1 - \beta)\Sigma^{-1} + \beta \left[\sum_i \mathbf{J}_\mu(\mathbf{x}_i)^\top \Lambda_\mu(\mathbf{x}_i) \mathbf{J}_\mu(\mathbf{x}_i) \right], \quad (48)$$

$$\mu \leftarrow \mu - \beta \Sigma \left[\frac{N}{\tau} \nabla_\mu \bar{\ell}_t(\mu) + \sum_{s=1}^{t-1} [\nabla_\mu \mathbf{m}_{t,s}] \mathbf{K}_{t-1,s}^{-1} (\mathbf{m}_{t,s} - \mathbf{m}_{t-1,s}) \right]. \quad (49)$$

Approximation 5: Similarly to Equation 36-37, our final approximation is to use a diagonal covariance Σ and replace the above update by an RMSprop-like update where we denote μ by \mathbf{w} :

$$\mathbf{s}^{-1} \leftarrow (1 - \beta)\mathbf{s} + \beta \left[\sum_i \Lambda_w(\mathbf{x}_i) [\mathbf{J}_w(\mathbf{x}_i) \circ \mathbf{J}_w(\mathbf{x}_i)]^\top \right], \quad (50)$$

$$\mathbf{w} \leftarrow \mathbf{w} - \beta \frac{1}{\mathbf{s} + \delta \mathbf{1}} \circ \left[\frac{N}{\tau} \nabla_w \bar{\ell}_t(\mathbf{w}) + \sum_{s=1}^{t-1} [\nabla_w \mathbf{m}_{t,s}] \mathbf{K}_{t-1,s}^{-1} (\mathbf{m}_{t,s} - \mathbf{m}_{t-1,s}) \right], \quad (51)$$

where we have added a regulariser δ to \mathbf{s} in the second line to avoid dividing by zero. Previously (Khan et al., 2018), this regulariser was the prior precision. Ideally, when using a functional prior, we would replace this by another term. However, this term was ignored by making Approximation 4, and we use δ instead. The final Gaussian approximation is obtained with the mean equal to \mathbf{w} and covariance is equal to a diagonal matrix with $1/(\mathbf{s} + \delta \mathbf{1})$ as its diagonal.

It is easy to see that the solutions found by this algorithm is the fixed point of this objective:

$$\min_{\mathbf{w}} N \bar{\ell}_t(\mathbf{w}) + \tau \sum_{s=1}^{t-1} (\mathbf{m}_{t,s} - \mathbf{m}_{t-1,s})^\top \mathbf{K}_{t-1,s}^{-1} (\mathbf{m}_{t,s} - \mathbf{m}_{t-1,s}), \quad (52)$$

Ultimately, this is an approximation of the objective given in Equation 39, and is computationally cheaper to optimise.

We follow the recommendations of Khan et al. (2019) and use RMSprop/Adam instead of Equation 34-35. This algorithm still optimises the objective given in Equation 52, but the estimate of the covariance is not accurate. We correct the approximation after convergence of the algorithm by recomputing the diagonal of the covariance according to Equation 50. Denoting the converged solution by \mathbf{w}_* , we compute the diagonal \mathbf{v}_* of the covariance Σ_* as shown below:

$$\mathbf{v}_* = \mathbf{1} / \left[\delta \mathbf{1} + \sum_{i=1}^N \Lambda_{w_*}(\mathbf{x}_i) [\mathbf{J}_{w_*}(\mathbf{x}_i) \circ \mathbf{J}_{w_*}(\mathbf{x}_i)]^\top \right], \quad (53)$$

C. Multiclass setting

When there are more than two classes per task, we can no longer use Equations 11-16 directly. Instead, we use their multiclass versions. We still make the same approximations as described in Appendix B.

Reducing Complexity in the Multiclass setting: We could use the full multiclass version of the GP predictive (Equation 29), but this is expensive. To keep computational complexity low, we employ an individual GP over each of the K classes seen in a previous task, and treat the GPs as independent.

We have K separate GPs. Let $\mathbf{y}^{(k)}$ be the k -th item of \mathbf{y} . Then the predictive distribution over each $\mathbf{y}^{(k)}$ for an input \mathbf{x} is:

$$\hat{p}(\mathbf{y}^{(k)} | \mathbf{x}, \mathcal{D}) := \mathcal{N}(\mathbf{y}^{(k)} | \mathcal{S}(\mathbf{f}_{w_*}(\mathbf{x}))^{(k)}, \Lambda_{w_*}(\mathbf{x})^{(k)} \mathbf{J}_{w_*}(\mathbf{x}) \Sigma_* \mathbf{J}_{w_*}(\mathbf{x})^\top \Lambda_{w_*}(\mathbf{x})^{(k)\top} + \Lambda_{w_*}(\mathbf{x})^{(k,k)}), \quad (54)$$

where $\mathcal{S}(\mathbf{f}_{w_*}(\mathbf{x}))^{(k)}$ is the k -th output of the softmax function, $\Lambda_{w_*}(\mathbf{x})^{(k)}$ is the k -th row of the Hessian matrix and $\Lambda_{w_*}(\mathbf{x})^{(k,k)}$ is the k, k -th element of the Hessian matrix. The Jacobians $\mathbf{J}_{w_*}(\mathbf{x})$ are now of size $K \times P$. Note that we have allowed \mathcal{S} and $\Lambda_{w_*}(\mathbf{x})$ to be of size K instead of $K - 1$. This is because we are treating the K GPs separately.

The kernel matrix \mathbf{K}_{t-1} is now a block diagonal matrix for each previous task's classes. This allows us to only compute inverses of each block diagonal (size $M \times M$), repeated for each class in each past task ($K(t - 1)$ times), where M is the

number of memorable past examples in each task. This changes computational complexity to be linear in the number of classes per task, K , compared to Section 3.5 (which has analysis for binary classification for each task).

When choosing a memorable past (the subset of points to regularise function values over) for the logistic regression case, we can simply sort the $\Lambda_{w_s}(\mathbf{x}_i)$'s for all $\{\mathbf{x}_i\} \in \mathcal{D}_t$ and pick the largest, as explained in Section 3.2. In the multiclass case, these are now $K \times K$ matrices $\Lambda_{w_s}(\mathbf{x}_i)$. We instead sort by $\text{Tr}(\Lambda_{w_s}(\mathbf{x}_i))$ to select the memorable past examples.

FROMP for multiclass classification: The solutions found by the multiclass algorithm is the fixed point of this objective (compare with Equation 52):

$$\min_{\mathbf{w}} N\bar{\ell}_t(\mathbf{w}) + \tau \sum_{s=1}^{t-1} \sum_{k \in C_s} (\mathbf{m}_{t,s,k} - \mathbf{m}_{t-1,s,k})^\top \mathbf{K}_{t-1,s,k}^{-1} (\mathbf{m}_{t,s,k} - \mathbf{m}_{t-1,s,k}), \quad (55)$$

where we define C_s as the set of classes k seen in previous task s , $\mathbf{m}_{t,s,k}$ is the vector of $m_{w_t}(\mathbf{x})$ for class k evaluated at the memorable points $\{\mathbf{x}_i\} \in \mathcal{M}_s$, $\mathbf{m}_{t-1,s,k}$ is the vector of $m_{w_{t-1}}(\mathbf{x})$ for class k , and $\mathbf{K}_{t-1,s,k}$ is the kernel matrix from the previous task just for class k , always evaluated over just the memorable points from previous task s . By decomposing the last term over individual outputs and over the memorable past from each task, we have reduced the computational complexity per update.

D. Functional prior approximation

We discuss why replacing weight space integral by a function space integral, as done below, results in an approximation:

$$\mathbb{E}_{q(\mathbf{w})}[\log q_{t-1}(\mathbf{w})] \approx \mathbb{E}_{\tilde{q}_{w_t}(\mathbf{f})}[\log \tilde{q}_{w_{t-1}}(\mathbf{f})],$$

A change of variable in many cases results in an equality, e.g., for $\mathbf{f} = \mathbf{X}\mathbf{w}$ with a matrix \mathbf{X} and given any function $h(\mathbf{f})$, we can express the weight space integral as the function space integral:

$$\int h(\mathbf{X}\mathbf{w}) \mathcal{N}(\mathbf{w}|\boldsymbol{\mu}, \boldsymbol{\Sigma}) d\mathbf{w} = \int h(\mathbf{f}) \mathcal{N}(\mathbf{f}|\mathbf{X}\boldsymbol{\mu}, \mathbf{X}\boldsymbol{\Sigma}\mathbf{X}^\top) d\mathbf{f}. \quad (56)$$

Unfortunately, $\log q_{t-1}(\mathbf{w})$ can not always be written as a function of $\mathbf{f} := \mathbf{J}_{w_t} \mathbf{w}$. Therefore, the change of variable does not result in an equality. For our purpose, as long as the approximations provide a reasonable surrogate for optimisation, the approximation is not expected to cause issues.

E. Further details on continual learning metrics reported

We report a backward transfer metric and a forward transfer metric on Split CIFAR (higher is better for both). The backward transfer metric is exactly as defined in Lopez-Paz & Ranzato (2017). The forward transfer metric is a measure of how well the method uses previously seen knowledge to improve classification accuracy on newly seen tasks. Let there be a total of T tasks. Let $R_{i,j}$ be the classification accuracy of the model on task t_j after training on task t_i . Let R_i^{ind} be the classification accuracy of an independent model trained only on task i . Then,

$$\begin{aligned} \text{Backward Transfer, BWT} &= \frac{1}{T-1} \sum_{i=1}^{T-1} R_{T,i} - R_{i,i}, \\ \text{Forward Transfer} &= \frac{1}{T-1} \sum_{i=2}^T R_{i,i} - R_i^{\text{ind}}. \end{aligned}$$

F. Further details on image experiments

F.1. Permuted MNIST

We use the Adam optimiser (Kingma & Ba, 2015) with Adam learning rate set to 0.001 and parameter $\beta_1 = 0.99$, and also employ gradient clipping. The minibatch size is 128, and we learn each task for 10 epochs. We use $\tau = N$ for all algorithms: FROMP, FRORP, FROMP- L_2 and FRORP- L_2 . We use a fully connected single-head network with two hidden layers, each consisting of 100 hidden units with ReLU activation functions. We report performance after 10 tasks.

F.2. Split MNIST

We use the Adam optimiser (Kingma & Ba, 2015) with Adam learning rate set to 0.0001 and parameter $\beta_1 = 0.99$, and also employ gradient clipping. The minibatch size is 128, and we learn each task for 15 epochs. We find good settings of τ to be $\tau = N$ for FROMP and FRORP, and $\tau = 0.1N$ for FROMP- L_2 and FRORP- L_2 . We use a fully connected multi-head network with two hidden layers, each with 256 hidden units and ReLU activation functions.

Smaller network architecture from Swaroop et al. (2019). Swaroop et al. (2019) use a smaller network than the network we use for the results in Table 1. They train VCL on a single-hidden layer network with 100 hidden units (and ReLU activation functions). To ensure faithful comparison, we reran FROMP (with 40 memorable points per task) on this smaller network, obtaining a mean and standard deviation over 5 runs of $99.2\% \pm 0.1$. This is an improvement from Table 1, which uses a larger network. We believe this is due to the pruning effect described in Swaroop et al. (2019).

Sensitivity to the value of τ . We tested FROMP and FROMP- L_2 with different values of the hyperparameter τ . We found that τ can change by an order of magnitude without significantly affecting final average accuracy. Larger changes in τ led to greater than 0.1% loss in accuracy.

F.3. Split CIFAR

We use the Adam optimiser (Kingma & Ba, 2015) with Adam learning rate set to 0.001 and parameter $\beta_1 = 0.99$, and also employ gradient clipping. The minibatch size is 256, and we learn each task for 80 epochs. We find good settings of τ to be $\tau = 10N$ for FROMP and FRORP, and $\tau = 20N$ for FROMP- L_2 and FRORP- L_2 .

Numerical results on Split CIFAR. We run all methods 5 times and report the mean and standard error. For baselines, we train from scratch on each task and jointly on all tasks achieving $73.6\% \pm 0.4$ and $78.1\% \pm 0.3$, respectively. The final average validation accuracy of FROMP is $76.2\% \pm 0.4$, FROMP- L_2 is $74.6\% \pm 0.4$, SI is $73.5\% \pm 0.5$ (result from Zenke et al. (2017)), EWC is $71.6\% \pm 0.9$, VCL + random coreset is $67.4\% \pm 1.4$.

F.4. Fewer memorable past examples

When we have fewer memorable past examples (for Figures 3 and 5b), we increase τ to compensate for the fewer datapoints. For example, for permuted MNIST, when we have 40 memorable past examples per task (instead of 200), we use $\tau = (200/40)N = 5N$ (instead of $\tau = N$ for 200 memorable past points).

G. Further toy data experiments

This section provides further information and visualisations of toy 2D datasets, as well as hyperparameter settings for VCL. We investigate the inconsistent behaviour of weight-space methods (VCL) on these toy datasets, and show that our functional-regularisation method is much more consistent, even across many different dataset variations.

G.1. Weight-space regularisation’s inconsistent behaviour

Table 2. Train accuracy of FROMP, VCL (no coresets), VCL+coresets and batch-trained Adam (an upper bound on performance) on a toy 2D binary classification dataset, with mean and standard deviations over 5 runs for VCL and batch Adam, and 10 runs for FROMP. ‘VCL’ is without coresets. VCL-RP and FRORP have the same (random) coreset selections. VCL-MP is provided with ‘ideal’ coreset points as chosen by an independent run of FROMP. VCL (no coreset) does very poorly, forgetting previous tasks. VCL+coresets is brittle with high standard deviations, while FROMP is stable.

FROMP	FRORP	VCL-RP	VCL-MP	VCL	Batch Adam
$99.6\% \pm 0.2$	$98.5\% \pm 0.6$	$92\% \pm 10$	$85\% \pm 14$	$68\% \pm 8$	$99.70\% \pm 0.03$

Table 2 summarises the performance (measured by train accuracy) of FROMP and VCL+coresets on a toy dataset similar to that in Figure 2. FROMP is very consistent, while VCL (with coresets) is extremely brittle: it can perform well sometimes (1 run out of 5), but usually does not (4 runs out of 5). This is regardless of the coreset points chosen for VCL. Note that coresets are chosen independently of training in VCL. Without coresets, VCL forgets many past tasks, with very low performance.

For VCL-MP, the coreset is chosen as the memorable past from an independent run of FROMP, with datapoints all on the task boundary. This selection of coreset is intuitively better than a random coreset selection. The results we show here are not specific to coreset selection. Any coreset selection (whether random or otherwise) all show the same inconsistency when VCL is trained with them.

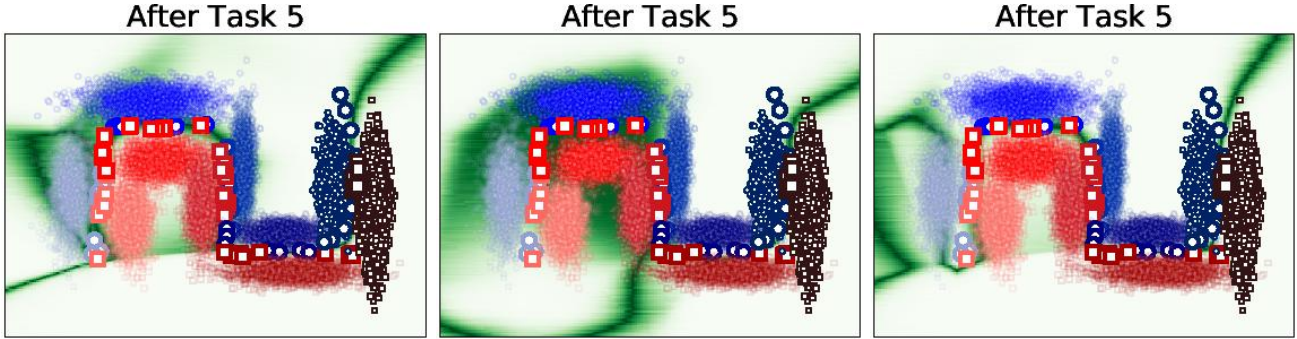


Figure 6. Three runs of VCL-MP on toy 2D data. These are the middle performing 3 runs out of 5 runs with different random seeds. VCL’s inconsistent behaviour is clear.

G.2. Dataset variations

Table 3. Train accuracy of FROMP and batch-trained Adam (upper bound on performance) on variations of a toy 2D binary classification dataset, with mean and standard deviations over 10 runs (3 runs for Adam). FROMP performs well across variations. VCL (with coresets) performs significantly worse even on the original dataset ($92\% \pm 10$). See Appendix G.2 for further experiments and for visualisations.

Dataset variation	FROMP	Batch Adam
Original dataset	$99.6\% \pm 0.2$	$99.7\% \pm 0.0$
10x less data (400 per task)	$99.9\% \pm 0.0$	$99.7\% \pm 0.2$
10x more data (40000 per task)	$96.9\% \pm 3.0$	$99.7\% \pm 0.0$
Introduced 6th task	$97.8\% \pm 3.3$	$99.6\% \pm 0.1$
Increased std dev of each class distribution	$96.0\% \pm 2.4$	$96.9\% \pm 0.4$
2 tasks have overlapping data	$90.1\% \pm 0.8$	$91.1\% \pm 0.3$

Figures 7 to 11 visualise the different dataset variations presented in Table 3. We pick the middle performing FROMP run (out of 5) and batch Adam run to show.

G.3. VCL and FROMP hyperparameter settings for toy datasets

FROMP. We optimised the number of epochs, Adam learning rate, and batch size. We optimised by running different hyperparameter settings for 5 runs on the toy dataset in Figure 2, and picking the settings with largest mean train accuracy. We found the best settings were: number of epochs=50, batch size=20, learning rate=0.01. The hyperparameters were then fixed across all toy data experimental runs, including across dataset variations (number of epochs was appropriately scaled by 10 if dataset size was scaled by 10).

VCL+coresets. We optimised the number of epochs, the number of coreset epochs (because VCL+coresets trains on non-coreset data first, then on coreset data just before test-time: see Nguyen et al. (2018)), learning rate (we use Adam to optimise the means and standard deviations of each parameter), batch size, and prior variance. We optimised by running various settings for 5 runs and picking the settings with largest mean train accuracy. We found the best settings were: number of epochs=200, number of coreset epochs=200, a standard normal prior (variance=1), batch size=40, learning rate=0.01. VCL is slow to run (an order of magnitude longer) compared to the other methods (FROMP and batch Adam).

H. Author Contributions Statement

List of Authors: Pingbo Pan, Siddharth Swaroop, Alexander Immer, Runa Eschenhagen, Richard E. Turner, Mohammad Emtiyaz Khan.

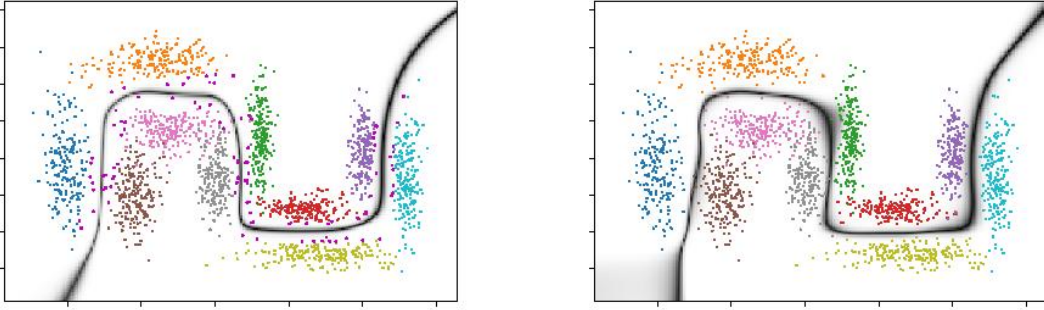


Figure 7. FROMP (middle performing of 5 runs) and batch Adam on a dataset 10x smaller (400 points per task).

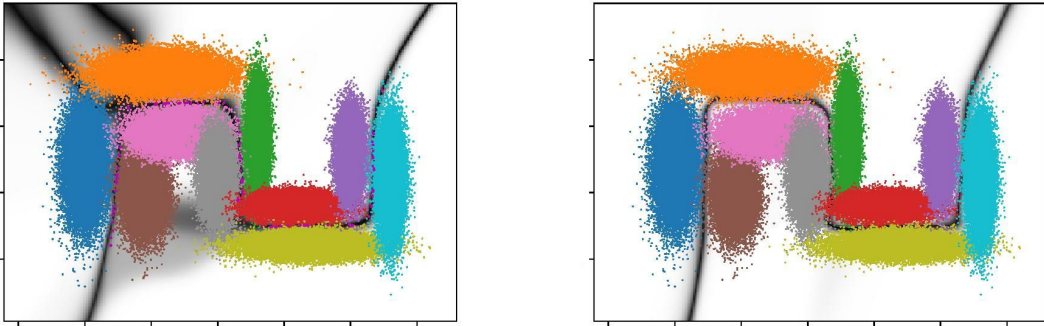


Figure 8. FROMP (middle performing of 5 runs), left, and batch Adam, right, on a dataset 10x larger (40,000 points per task).

P.P, S.S., and M.E.K. conceived the original idea of using DNN2GP for continual learning. This was then discussed with R.E., R.T., and A.I. The DNN2GP result from Section 3.1 is due to A.I. The memorable past method in Section 3.2 is due to M.E.K. The FROMP algorithm in Algorithm 1 was originally conceived by P.P., S.S. and M.E.K. The idea of functional prior was conceived by S.S. and M.E.K. Based on this idea, S.S. and M.E.K. wrote a derivation using the variational approach, which is currently written in Section 3.3. R.E., A.I. and R.T. regularly provided feedback for the main methods.

P.P. conducted all experiments, with feedback from M.E.K., A.I., R.E. and S.S. S.S. made corrections to some of the code, fixed hyperparameter reporting, and also did baseline comparisons.

The first version of the paper was written by M.E.K. with some help from the other authors. S.S. revised the paper many times and also rewrote many new parts. Detailed derivation in Appendix is written by S.S. and M.E.K. The authors A.I., R.E. and R.T. provided feedback during the writing of the paper.

M.E.K. and S.S. led the project.

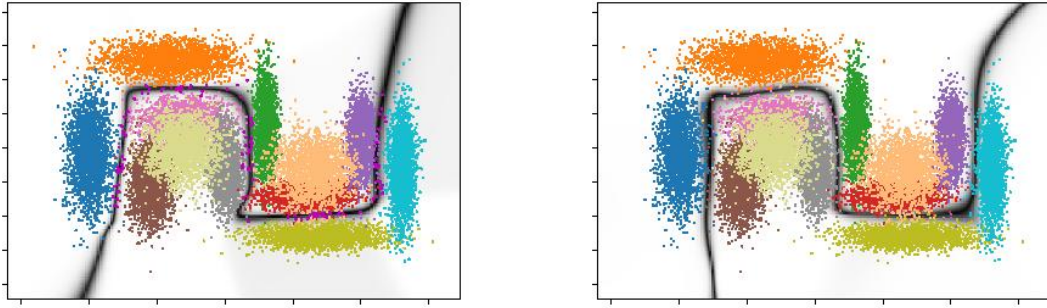


Figure 9. FROMP (middle performing of 5 runs), left, and batch Adam, right, on a dataset with a new, easy, 6th task.

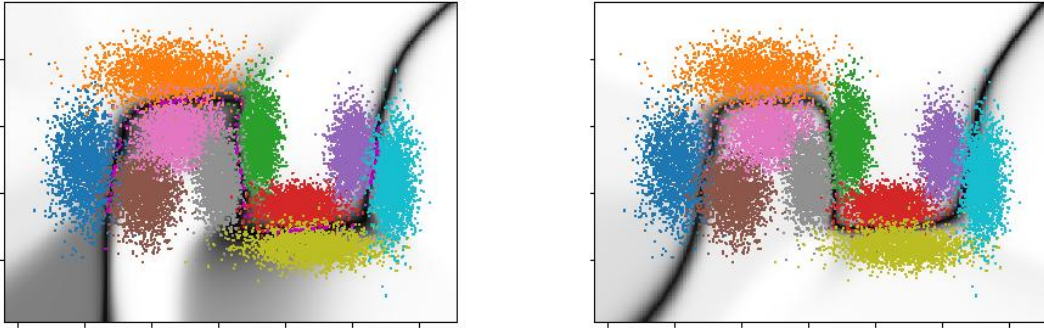


Figure 10. FROMP (middle performing of 5 runs), left, and batch Adam, right, on a dataset with increased standard deviations of each class' points, making classification tougher.

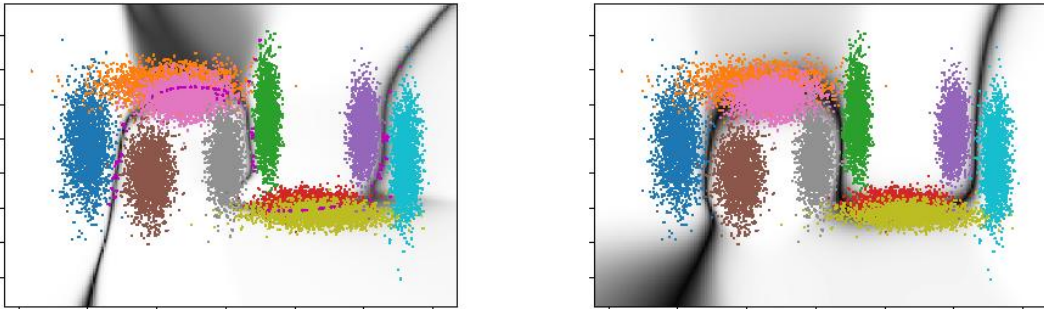


Figure 11. FROMP (middle performing of 5 runs), left, and batch Adam, right, on a dataset with 2 tasks having overlapping data, which is not separable.